29. Rosenfeldt H, Vázquez-Prado J, Gutkind JS (2004) P-REX2, a novel PI-3-kinase sensitive Rac exchange factor. FEBS Lett 572: 167-171. doi:10.1016/j.febslet.2004.06.097. PubMed: 15304342.
30. Das B, Shu X, Day GJ, Han J, Krishna UM et al. (2000) Control of intramolecular interactions between the pleckstrin homology and Dbl homology domains of Vav and Sos1 regulates Rac binding. J Biol Chem 275: 15074-15081. doi:10.1074/jbc.M907269199. PubMed: 10748082.
31. Hill K, Krugmann S, Andrews SR, Coadwell WJ, Finan P et al. (2005) Regulation of P-Rex1 by phosphatidylinositol (3,4,5)-trisphosphate and Gbetagamma subunits. J Biol Chem 280: 4166-4173. PubMed: 15545267.
32. Chhatriwala MK, Betts L, Worthylake DK, Sondek J (2007) The DH and PH domains of Trio coordinately engage Rho GTPases for their efficient activation. J Mol Biol 368: 1307-1320. doi:10.1016/j.jmb.2007.02.060. PubMed: 17391702.
33. Sosa MS, Lopez-Haber C, Yang C, Wang H, Lemmon MA et al. (2010) Identification of the Rac-GEF P-Rex1 as an essential mediator of ErbB signaling in breast cancer. Mol Cell 40: 877-892. doi:10.1016/j.molcel.2010.11.029. PubMed: 21172654.
34. Kanehisa M, Goto S, Furumichi M, Tanabe M, Hirakawa M (2010) KEGG for representation and analysis of molecular networks involving diseases and drugs. Nucleic Acids Res 38: D355-D360. doi:10.1093/nar/gkp896. PubMed: 19880382.
35. Hecht JL, Mutter GL (2006) Molecular and pathologic aspects of endometrial carcinogenesis. J Clin Oncol 24: 4783-4791. doi:10.1200/JCO.2006.06.7173. PubMed: 17028294.
36. Li C, Fang R, Sun Y, Han X, Li F et al. (2011) Spectrum of oncogenic driver mutations in lung adenocarcinomas from East Asian never smokers. PLOS ONE 6: e28204. doi:10.1371/journal.pone.0028204. PubMed: 22140546.
37. Shigematsu H, Lin L, Takahashi T, Nomura M, Suzuki M et al. (2005) Clinical and biological features associated with epidermal growth factor receptor gene mutations in lung cancers. J Natl Cancer Inst 97: 339-346. doi:10.1093/jnci/dji055. PubMed: 15741570.
38. Sharma SV, Bell DW, Settleman J, Haber DA (2007) Epidermal growth factor receptor mutations in lung cancer. Nat Rev Cancer 7: 169-181. doi:10.1038/nrc2088. PubMed: 17318210.
39. Bos JL (1989) ras oncogenes in human cancer: a review. Cancer Res 49: 4682-4689. PubMed: 2547513.
40. Degen M, Brellier F, Kain R, Ruiz C, Terracciano L et al. (2007) Tenascin-W is a novel marker for activated tumor stroma in low-grade human breast cancer and influences cell behavior. Cancer Res 67: 9169-9179. doi:10.1158/0008-5472.CAN-07-0666. PubMed: 17909022.
41. Degen M, Brellier F, Schenk S, Driscoll R, Zaman K et al. (2008) Tenascin-W, a new marker of cancer stroma, is elevated in sera of colon and breast cancer patients. Int J Cancer 122: 2454-2461. doi:10.1002/ijc.23417. PubMed: 18306355.
42. Brellier F, Martina E, Degen M, Heuzé-Vourc'h N, Petit A et al. (2012) Tenascin-W is a better cancer biomarker than tenascin-C for most human solid tumors. BMC Clin Pathol 12: 14. doi:10.1186/1472-6890-12-14. PubMed: 22947174.
43. Dasika GK, Lin SC, Zhao S, Sung P, Tomkinson A et al. (1999) DNA damage-induced cell cycle checkpoints and DNA strand break repair in development and tumorigenesis. Oncogene 18: 7883-7899. PubMed: 10630641.
44. Bartkova J, Horejsi Z, Koed K, Kramer A, Tort F et al. (2005) DNA damage response as a candidate anti-cancer barrier in early human tumorigenesis. Nature 434: 864-870. doi:10.1038/nature03482. PubMed: 15829956.
45. Yan X, Baxter RC, Firth SM (2010) Involvement of pregnancy-associated plasma protein-A2 in insulin-like growth factor (IGF) binding protein-5 proteolysis during pregnancy: a potential mechanism for increasing IGF bioavailability. J Clin Endocrinol Metab 95: 1412-1420. doi:10.1210/jc.2009-2277. PubMed: 20103653.
46. Overgaard MT, Boldt HB, Laursen LS, Sottrup-Jensen L, Conover CA et al. (2001) Pregnancy-associated plasma protein-A2 (PAPP-A2), a novel insulin-like growth factor-binding protein-5 proteinase. J Biol Chem 276: 21849-21853. doi:10.1074/jbc.M102191200. PubMed: 11264294.
47. Shimasaki S, Shimonaka M, Zhang HP, Ling N (1991) Identification of five different insulin-like growth factor binding proteins (IGFBPs) from adult rat serum and molecular cloning of a novel IGFBP-5 in rat and human. J Biol Chem 266: 10646-10653. PubMed: 1709938.
48. Su Y, Wagner ER, Luo Q, Huang J, Chen L et al. (2011) Insulin-like growth factor binding protein 5 suppresses tumor growth and metastasis of human osteosarcoma. Oncogene 30: 3907-3917. doi:10.1038/onc.2011.97. PubMed: 21460855.
49. Huang T, Jiang M, Kong X, Cai YD (2012) Dysfunctions associated with methylation, microRNA expression and gene expression in lung cancer. PLOS ONE 7: e43441. doi:10.1371/journal.pone.0043441. PubMed: 22912875.
50. Li H, Handsaker B, Wysoker A, Fennell T, Ruan J et al. (2009) The Sequence Alignment/Map format and SAMtools. Bioinformatics 25: 2078-2079. doi:10.1093/bioinformatics/btp352. PubMed: 19505943.
51. Fujimoto A, Nakagawa H, Hosono N, Nakano K, Abe T et al. (2010) Whole-genome sequencing and comprehensive variant analysis of a Japanese individual using massively parallel sequencing. Nat Genet 42: 931-936. doi:10.1038/ng.691. PubMed: 20972442.
52. Quevillon E, Silventoinen V, Pillai S, Harte N, Mulder N et al. (2005) InterProScan: protein domains identifier. Nucleic Acids Res 33: W116-W120. doi:10.1093/nar/gni118. PubMed: 15980438.

Cancer Science
Japanese Cancer Association JCA
Open Access

Effect of a poly(ADP-ribose) polymerase-1 inhibitor against esophageal squamous cell carcinoma cell lines

Tomomitsu Nasuno,[1,2] Sachiyo Mimaki,[1] Makito Okamoto,[2] Hiroyasu Esumi[1,3] and Katsuya Tsuchihara[1]

[1]Division of Translational Research, Exploratory Oncology Research and Clinical Trial Center, National Cancer Center, Kashiwa, Chiba; [2]Department of Otorhinolaryngology, University of Kitasato Hospital, Minami-ku, Sagamihara, Kanagawa; [3]Research Institute for Biological Sciences, Tokyo University of Science, Noda, Chiba, Japan

Key words

DNA repair, esophageal cancer, poly(ADP-ribose) polymerase inhibitor, RNF8, γ-H2AX

Correspondence

Katsuya Tsuchihara, Division of Translational Research, Exploratory Oncology Research and Clinical Trial Center, National Cancer Center, 6-5-1 Kashiwanoha, Kashiwa, Chiba 277-8577, Japan.
Tel: +81-4-7133-1111; Fax: +81-4-7134-8786;
E-mail: ktsuchih@east.ncc.go.jp

Funding information

National Cancer Center Research and Development Fund (23-A-8, 15). Third Term Comprehensive 10-year Strategy for Cancer Control from the Ministry of Health, Labour and Welfare (H22-033).

Received July 8, 2013; Revised November 5, 2013; Accepted November 11, 2013

Cancer Sci **105** (2014) 202–210

doi: 10.1111/cas.12322

Effective molecular target drugs that improve therapeutic efficacy with fewer adverse effects for esophageal cancer are highly anticipated. Poly(ADP-ribose) polymerase (PARP) inhibitors have been proposed as low-toxicity agents to treat double strand break (DSB)-repair defective tumors. Several findings imply the potential relevance of DSB repair defects in the tumorigenesis of esophageal squamous cell carcinoma (ESCC). We evaluated the effect of a PARP Inhibitor (AZD2281) on the TE-series ESCC cell lines. Of these eight cell lines, the clonogenic survival of one (TE-6) was reduced by AZD2281 to the level of DSB repair-defective Capan-1 and HCC1937 cells. AZD2281-induced DNA damage was implied by increases in γ-H2AX and cell cycle arrest at G2/M phase. The impairment of DSB repair in TE-6 cells was suggested by a sustained increase in γ-H2AX levels and the tail moment calculated from a neutral comet assay after X-ray irradiation. Because the formation of nuclear DSB repair protein foci was impaired in TE-6 cells, whole-exome sequencing of these cells was performed to explore the gene mutations that might be responsible. A novel mutation in RNF8, an E3 ligase targeting γ-H2AX was identified. Consistent with this, polyubiquitination of γ-H2AX after irradiation was impaired in TE-6 cells. Thus, AZD2281 induced growth retardation of the DSB repair-impaired TE-6 cells. Interestingly, a strong correlation between basal expression levels of γ-H2AX and sensitivity to AZD2281was observed in the TE-series cells (R^2 = 0.5345). Because the assessment of basal DSB status could serve as a biomarker for selecting PARP inhibitor-tractable tumors, further investigation is warranted.

Esophageal carcinoma is the sixth most common cause of cancer-related deaths worldwide and is associated with a poor prognosis.[1] Surgical therapies of resectable esophageal cancer exhibit a 5-year survival rate ranging from 20% to 27%.[2–4] Less invasive therapies that preserve the esophagus have also been introduced. Endoscopic therapies, such as endoscopic mucosal resection (EMR) and endoscopic submucosal dissection (ESD), have been adopted for early esophageal cancer and have achieved favorable outcomes, but postoperative esophageal stricture frequently occurs after these treatments. Furthermore, intensive follow-up is necessary to manage new heterochronous lesions.[5–7] Chemoradiotherapy (CRT), which combines radiation, 5-fluorouracil (5-FU) and cisplatin (CDDP), is a promising therapeutic alternative to esophagectomy with a survival rate equivalent to that of surgical therapies.[8,9] However, the acute and late adverse effects of chemoradiotherapy, including pancytopenia and pneumonitis, still require consideration. There is a demand for effective molecular target drugs for esophageal cancer that combine an improved therapeutic efficacy with fewer adverse effects.

Poly(ADP-ribose) polymerase (PARP) inhibitors induce the accumulation of DNA single-strand breaks (SSB), which cause the formation of DNA double-strand breaks (DSB) after the stalling and collapse of progressing DNA replication folks.[10] Though DSBs are repaired by the error-free homologous recombination repair (HRR) pathway in non-tumor cells, they remain unrepaired and induce lethality in HRR-defective tumor cells.[11,12] Based on this mechanism, PARP inhibitors have been proposed as low toxicity agents for HRR-defective tumors. BRCA1 and BRCA2 are key components of the HRR machinery, and the abnormality of these genes is known to cause sporadic and hereditary breast and ovarian cancers.[13] Consistent with this, PARP inhibitors have been developed for breast and ovarian cancers. In addition, an increasing number of biomarker candidates that predict the sensitivity of a tumor to PARP inhibitors have been reported.[14–18]

Esophageal carcinoma is histologically classified into squamous cell carcinoma (ESCC) and adenocarcinoma; the former is common in East Asia. Although the direct relevance has not been well investigated, several findings suggest that a defect in the HRR pathway contributes to the tumorigenesis of ESCC. The risk of esophageal and head and neck squamous carcinoma is increased among Fanconi anemia (FA)

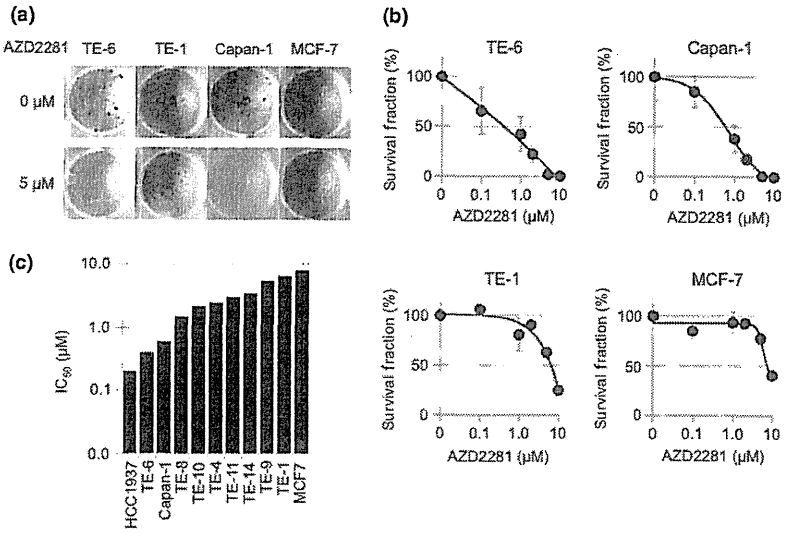

Fig. 1. Sensitivity of TE-series cell lines to a poly (ADP-ribose) polymerase (PARP) inhibitor, AZD2281. (a) TE-1, TE-6, Capan-1 (BRCA2-deficient) and MCF7 (wild-type BRCA) cells were treated with or without AZD2281 at the indicated concentrations for at least seven doubling times. Cells were fixed and stained with crystal violet and the number of colonies was counted. (b) Sensitivity to AZD2281 was evaluated by clonogenic assay. Colonies consisting of more than 64 cells were counted and the survival fraction was estimated. Three independent experiments were carried out. The data represent the average and standard deviations. (c) IC_{50} (μM) value of AZD2281 in eight TE series, MCF7, HCC1937 and Capan-1 cells measured by the clonogenic assays.

patients whose HRR pathway was disturbed due to FA-predisposing gene alterations.[19,20] In addition, recently reported whole-exome sequencing data from 74 head and neck SCCs revealed that more than half of SCC cases harbored mutations in genes involved in DNA repair.[21] Therefore, we assume that some fraction of ESCCs harbor DSB repair defects and might be favorable targets of PARP inhibitors. The aim of this study was to examine the efficacy of a potent PARP-1 inhibitor in a series of ESCC cell lines established from Japanese patients.

Materials and Methods

Complete materials and methods were described in the supplementary information (Data S1).

Purchased materials. A PARP inhibitor, AZD2281 (Olaparib) and BSI-201 (Iniparib) were purchased from Selleck Chemicals (Houston, TX, USA). The TE-1, TE-4, TE-6, TE-8, TE-9, TE-10, TE-11 and TE-14 cell lines were purchased from the Riken BioResource Center (Tsukuba, Japan). The Capan-1, HCC1937, MDA-MB-436 and MCF-7 cell lines were purchased from the American Type Culture Collection (ATCC, Manassas, VA, USA).

Clonogenic assays. A total of 500–2000 cells were cultured with AZD2281- or vehicle-containing media. After 10–16 days, cells were fixed and stained with crystal violet. Colonies consisting of more than 64 cells were subsequently counted.

Immunoblotting analysis. The treated cell lysates were separated by 15% SDS-PAGE and the blot was hybridized with the

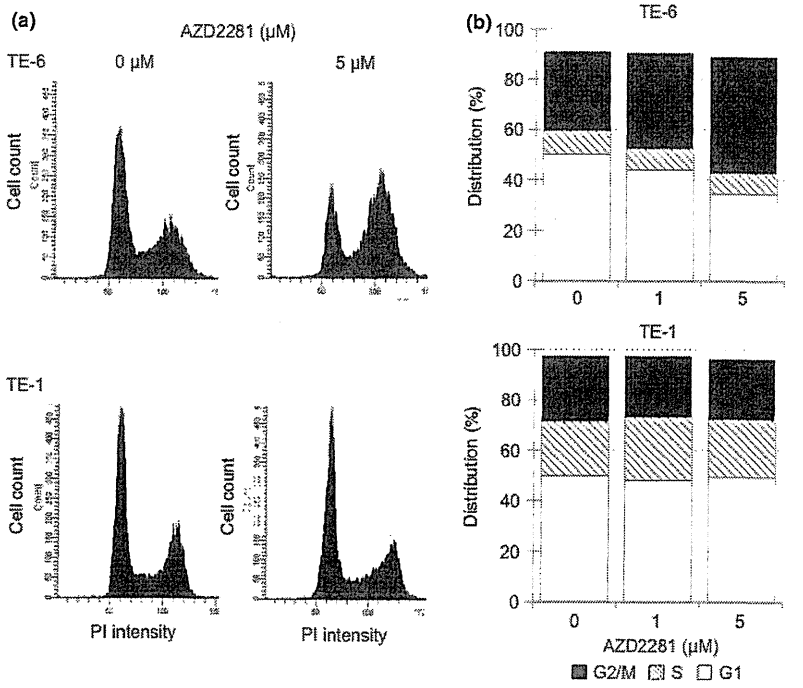

Fig. 2. AZD2281-induced G2/M arrest in TE-6 cells. (a) TE-6 and TE-1 cells were cultured with or without AZD2281 for 24 h. DNA ploidy was assessed by propidium iodide (PI) staining and flow cytometry. (b) The proportion of estimated cell-cycle phases in TE-6 and TE-1 cells treated with or without AZD2281. The data represent the average of three independent experiments.

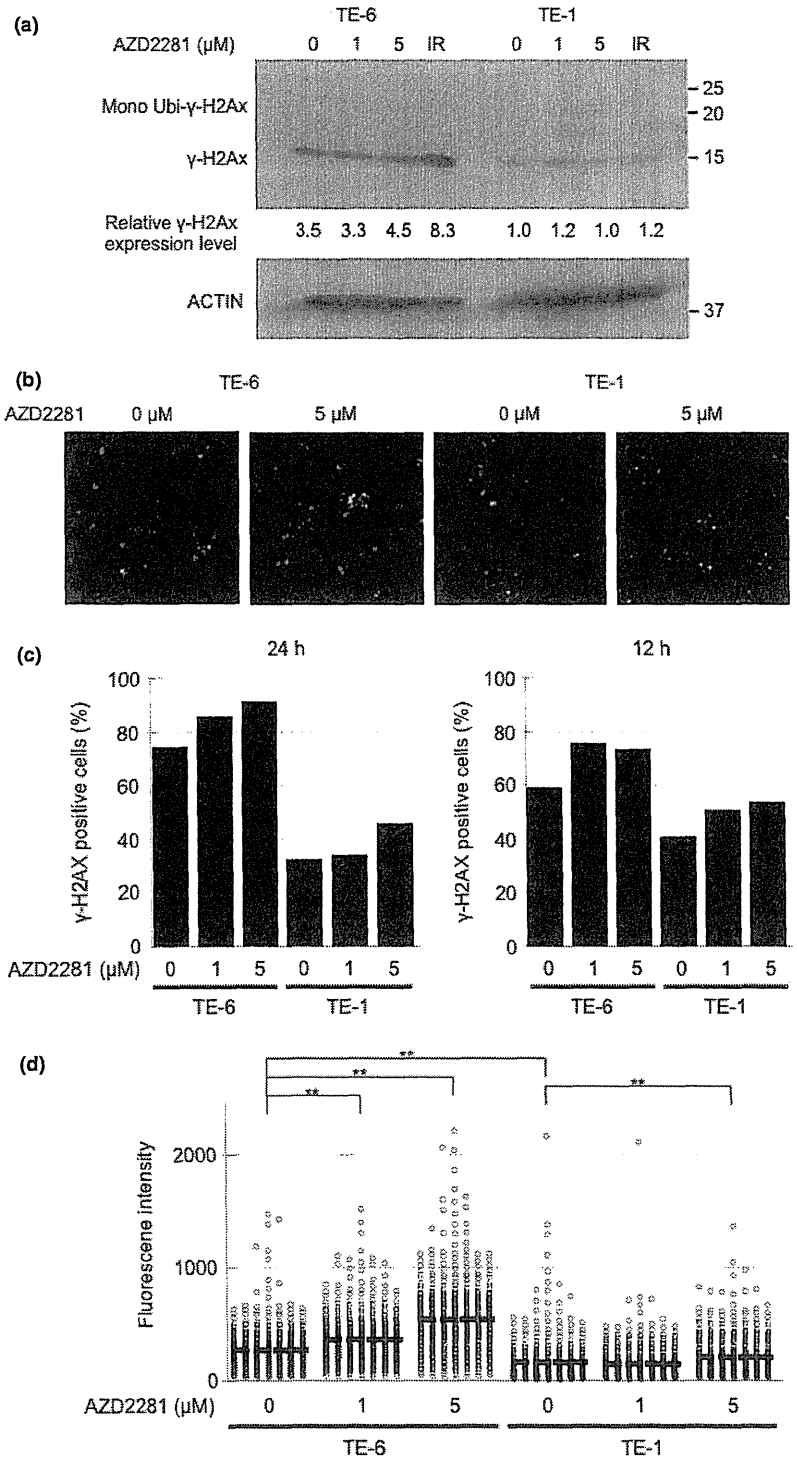

Fig. 3. Increase in double strand breaks (DSBs) in TE-6 cells treated with AZD2281. (a) TE-6 and TE-1 cells were treated with AZD2281 for 24 h and with 5 Gy X-ray irradiation, and γ-H2AX was assessed using Western blotting. The anti-γ-H2AX antibody detected both unubiquitinated (15 kD) and mono-ubiquitinated (23.6 kD) γ-H2AX. (b) TE-6 and TE-1 cells were treated with AZD2281 for 24 h and γ-H2AX was assessed by immunofluorescence. DAPI (blue) and γ-H2AX (red) images were superimposed. (c) Number of the γ-H2AX-positive TE-6 and TE-1 cells treated with or without AZD2281 at the indicated concentrations for 24 h. (d) Scatter diagrams show the fluorescence intensity of individual TE-6 and TE-1 cells treated with or without AZD2281 at the indicated concentrations for 24 h. The lines shown indicated the averages of the data plotted. The data were obtained from at least 500 cells for each condition. $^{**}P < 0.01$ (Student's *t*-test).

phospho-Histone H2A.X (Ser139) (20E3) rabbit monoclonal antibody (1:1000; Cell Signaling Technology, Danvers, MA, USA) and then with a HRP-conjugated secondary antibody (1:50000; Santa Cruz Biotechnology, Dallas, TX, USA). Densitometric analysis was performed with Image-J software (http://imagej.nih.gov/ij/).

Immunofluorescence analysis. To evaluate the formation of DSBs, cells grown on 96-well plates were treated with an anti-γ-H2AX rabbit monoclonal antibody (Cell Signaling Technology) followed by a goat anti-Mouse IgG (H + L) DyLight 549-conjugated secondary antibody (Thermo Scientific, Waltham, MA, USA). γ-H2AX was observed under an ArrayScan HCS System (Thermo Scientific). To evaluate the formation of 53BP1 and RAD51 nuclear foci, cells grown on μ-Dish$^{35\ mm,\ low}$ (ibidi) were treated with an anti-53BP1 rabbit polyclonal antibody (Abcam, Cambridge, UK) or an anti-RAD51 rabbit

polyclonal antibody (Santa Cruz Biotechnology) followed by an Alexa Flour 488 donkey anti-rabbit IgG (H + L) (Invitrogen, Carlsbad, CA, USA). These foci were observed under a BIOREVO BZ-9000 microscope (Keyence, Osaka, Japan).

Neutral comet assays. Neutral comet assays were performed using the CometAssay kit (Trevigen, Gaithersburg, MD, USA) according to the manufacturer's instructions.

Cell cycle analysis. The cells were fixed with 70% ethanol and stained with propidium iodide. The DNA content of the cells was evaluated using a FACS CantoII flow cytometer and FACS Diva software (BD, Franklin Lakes, NJ, USA).

Whole-exome sequencing. Targeted enrichment was performed using the SureSelect Human All Exon 50 Mb Kit (Agilent Technologies, Santa Clara, CA, USA) and sequenced using Illumina Genome Analyzer IIx (Illumina, San Diego, CA, USA).

Statistical analysis. Individual experiments were performed at least in triplicate. The statistical significance of observed differences was analyzed using Student's *t*-test. One asterisk (*) indicates a *P*-value smaller than 0.05. Two asterisks (**) indicate a *P*-value smaller than 0.01.

Results

Sensitivity of TE series cell lines to AZD2281. We tested the sensitivity of the TE series of ESCC cell lines to AZD2281 using clonogenic assays. All of the cell lines were cultured with various concentrations of AZD2281 for at least seven doubling times (10–16 days), and the number of colonies with more than 64 cells was counted. The concentrations of AZD2281 that caused a 50% reduction in clonogenic survival (IC_{50}) in the TE-6, TE-8, TE-10, TE-4, TE-11, TE-14, TE-9, and TE-1 cells were 0.4, 1.5, 2.2, 2.5, 3.0, 3.5, 5.5 and 6.5 μM, respectively (Figs 1a–c, S1). The IC_{50} values for HCC1937 and Capan-1 cells, which have deletions or mutations in the BRCA genes and are reported to be sensitive to PARP inhibitors,[22,23] were 0.2 and 0.6 μM, respectively. The IC_{50} values for MCF7 cells, which have wild-type BRCA genes and are known to be resistant to PARP inhibitors, was 8.0 μM. We further tested another PARP inhibitor, BSI-201. The IC_{50} values for TE-6 and TE- 1 cells were 9.6 and 22.0 μM, respectively (Fig. S2). Because AZD2281 and BSI-201 suppressed the growth of the TE-6 cells as efficiently as it suppressed the growth of the BRCA-deficient, PARP-inhibitor-sensitive cell lines and failed to suppress the growth of the TE-1 cells; we designated TE-6 as a PARP inhibitor-sensitive ESCC cell line and TE-1 as a PARP inhibitor-resistant cell line. We selected these cells for further analyses.

AZD2281-induced G2/M arrest in TE-6 cells. To further study the mechanism of growth retardation of TE-6 cells by AZD2281, the status of the cell cycle in these cells was assessed by analyzing the DNA ploidy pattern (Figs 2a,b, S3). Treatment with 1 and 5 μM of AZD2281 for 12 h increased the population with 4n DNA content from 36.7% to 40.7% and 40.6%, respectively. Treatment for 24 h further increased the population with 4n DNA content from 31.6% to 37.9% and 46.3%, respectively. This suggested an increase in the G2/M or M arrested population after AZD2281 treatment. On the other hand, no significant increase of tetraploid cells was observed in the TE-1 cells.

Increase of DSBs in TE-6 cells treated with AZD2281. To determine whether DSBs are formed after treatment with AZD2281 for 24 h, we assessed the amount of γ-H2AX as a marker of DSBs. Western blotting revealed that the level of γ-H2AX staining in TE-6 cells increased in a dose-dependent manner. However, no such increase was observed in TE-1 cells (Fig. 3a). The same trend was observed by immunofluorescence. Both the percentage of γ-H2AX positive cells determined by visual inspection and the average fluorescence intensity of γ-H2AX staining per cell increased significantly in a dose-dependent manner in TE-6 cells, but not in TE-1 cells, suggesting that AZD2281 induced an accumulation of DNA damage in TE-6 cells (Fig. 3b–d).

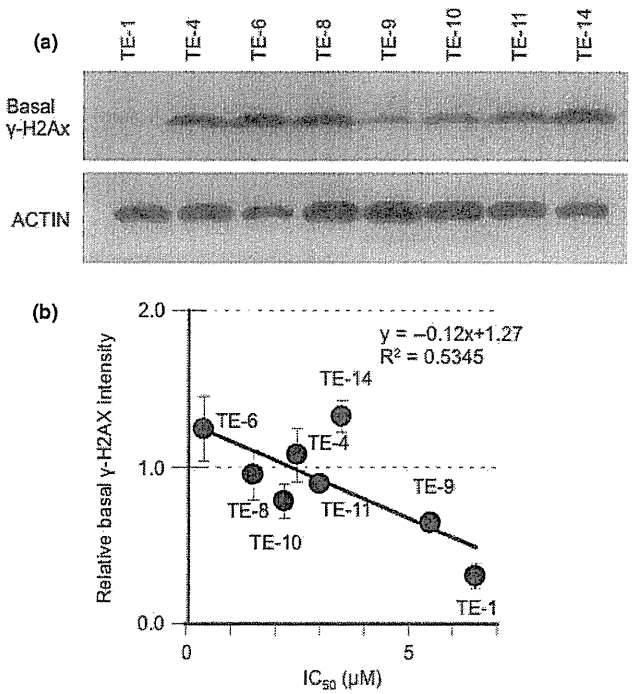

Fig. 4. A strong correlation between base-level γ-H2AX and sensitivity to AZD2281 of TE cells. (a) Eight non-treated TE-series cell lines were subjected to Western blot analysis with antibodies against γ-H2AX and actin. (b) The correlation between basal γ-H2AX expression levels and IC50 of AZD2281. The average intensity of γ-H2AX was standardized with actin. The data represent the averages and standard deviations of three independent experiments.

A strong correlation between base-level γ-H2AX and sensitivity to AZD2281 of TE cells. The Western blotting and immunofluorescence data also suggested that the baseline γ-H2AX level was higher in the AZD2281-sensitive TE-6 cells than in the resistant TE-1 cells (Fig. 3a). Because the increased amount of γ-H2AX may suggest the accumulation of DSBs, we evaluated the correlation between the basal expression levels of γ-H2AX and sensitivity to AZD2281 among the eight TE cell lines. A significant correlation between the basal levels of γ-H2AX and the IC_{50} of AZD2281 was observed ($R^2 = 0.5345$) (Fig. 4a,b).

Sustained X-ray irradiation-induced DSBs in TE-6 cells. To assess whether the impairment of DSB repair is relevant to the sensitivity of TE-series cells to AZD2281, we evaluated X-ray

Table 1. Tail moment of the X-ray-irradiated TE-6 and TE-1 cells

	Time after irradiation			
	0 h	15 min	2 h	6 h
TE-6	2.43 ± 3.19	5.27 ± 4.35	9.78 ± 6.27	13.7 ± 8.20
TE-1	3.69 ± 4.14	5.56 ± 3.97	5.20 ± 4.22	3.20 ± 4.71

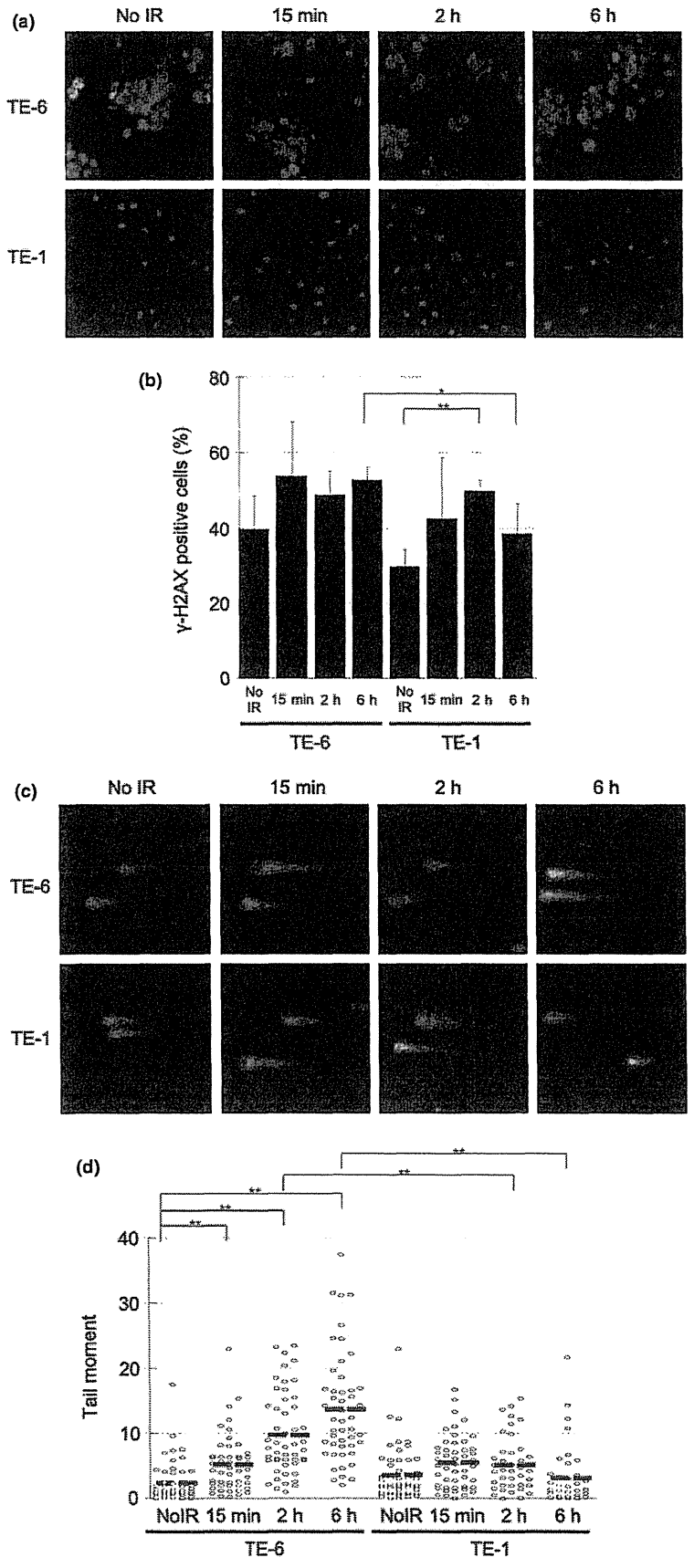

Fig. 5. Sustained X-ray irradiation-induced double strand breaks (DSBs) in TE-6 cells. (a) TE-6 and TE-1 cells were irradiated with 2 Gy X-ray. Cells were stained with anti-γ-H2AX antibody 15 min, 2 and 6 h after irradiation. (b) Percentages of γ-H2AX-positive cells. The data represent the average and standard deviations of three independent experiments. $*P < 0.05$, $**P < 0.01$ (Student's *t*-test). (c) Representative neutral comet assay results of TE-6 and TE-1 cells treated with or without 5 Gy of X-ray irradiation. (d) Scatter diagrams show the tail moment of individual TE-6 and TE-1 cells treated with or without 5 Gy of X-ray irradiation. The lines shown indicate the averages of the data plotted. The data were obtained from at least 100 cells for each condition. $*P < 0.01$ (Student's *t*-test).

Table 2. The number of nuclear foci of the DNA repair proteins

X-Ray (Gy)	53BP1			Rad51	
	0	2		0	10
Time	–	15 min	2 h	–	2 h
TE-6	0.55 ± 1.44	0.94 ± 1.12	1.48 ± 1.20	0.67 ± 2.20	2.25 ± 3.20
TE-1	1.09 ± 1.58	2.48 ± 2.44	4.86 ± 3.23	1.11 ± 1.50	3.65 ± 3.59

irradiation-induced DNA DSBs in these cells. First, the amount of γ-H2AX was assessed by immunfluorescence. As mentioned above, the γ-H2AX level of TE-6 cells was high at baseline and increased 15 min after irradiation and sustained for 6 h. In TE-1 cells, increase of γ-H2AX level was observed 2 h after irradiation, but declined after 6 h (Fig. 5a,b). Next, a neutral comet assay was performed to assess DNA damage. This assay detects a wide range of DNA lesions, including DSBs; the tail moment parameter is used as an index of DNA damage. We found a sustained increase in the tail moment of TE-6 cells (irradiation [–]; 2.43 ± 3.19, 15 min; 5.27 ± 4.35 2 h; 9.78 ± 6.27, 6 h; 13.71 ± 8.20), while in TE-1 cells, the tail moment transiently increased at 2 h after 5 Gy X-ray irradiation and then returned to the basal level at 6 h (irradiation [–]; 3.69 ± 4.14, 15 min; 5.56 ± 3.97 2 h; 5.20 ± 4.22, 6 h; 3.20 ± 4.71) (Fig. 5c,d, Table 1). These results suggested that the X-ray irradiation-induced DNA damage was properly repaired in the TE-1 cells but was sustained in the TE-6 cells.

Impairment of DSB repair protein nuclear foci formation in X-ray irradiated TE-6 cells. Because the TE-6 cells were found to be defective in DSB repair, we assessed the amount of BRCA1/2 expression in TE-series cells by Western blotting (Fig. S4a,b). However, no significant difference in the expression of BRCA1/2 in TE-6 and TE-1 cells was observed. To confirm the impairment of DNA repair machinery of TE-6 cells, we evaluated the nuclear focus formation of 53BP1, which is recruited to the γ-H2AX sites at an early stage in DSB repair, and RAD51, which is recruited at a late stage in DSB repair.[24–26] The baseline expression levels of 53BP1 and RAD51 were higher in the TE-6 cells (Fig. S5). However, increase of the number of 53BP1 nuclear foci per cell was much less in the TE-6 cells (irradiation [–]; 0.55 ± 1.44, 15 min; 0.94 ± 1.12 2 h; 1.48 ± 1.20), whereas 53BP1 foci were increased in the TE-1 cells (irradiation [–]; 1.09 ± 1.58, 15 min; 2.48 ± 2.44 2 h; 4.86 ± 3.23) (Fig. 6a,b, Table 2). Similarly, 6 h after 10 Gy X-ray irradiation, the number of RAD51 foci per cell was significantly increased in the TE-1 cells (irradiation [–]; 1.11 ± 1.50, 6 h; 3.65 ± 3.59), whereas the increase in RAD51 foci was not significant in the TE-6 cells (irradiation [–]; 0.67 ± 2.20, 2 h; 2.25 ± 3.20) (Fig. 6c,d, Table 2). These results suggested that the interaction between γ-H2AX and 53BP1 and the subsequent recruitment of RAD51 were impaired in TE-6 cells.

A novel mutation in the *RNF8* gene, and the reduced ability of TE-6 cells to polyubiquitinate γ-H2AX. To identify the molecular mechanism underlying the impaired DNA repair in TE-6 cells, we performed whole-exome sequencing of TE-6 and TE-1 cells and selected the DNA repair-related genes that were mutated in the genomic DNA of TE-6 cells but not TE-1 cells. In total, 16 722 and 16 543 single nucleotide variants (SNV) were identified from the exomes of TE-1 and TE-6 cells, respectively (Tables S1 and S2). Another 260 and 240 indels were identified from TE-1 and TE-6 cells, respectively. To reduce the probable germline variants, the single nucleotide polymorphisms (SNPs) that were registered in the dbSNP and in-house Japanese SNP databases were eliminated. Finaly, 606 SNVs and 118 indels were exclusively identified in the TE-6 cells. Among these mutations were hits in six genes (listed in Table 3) that are related to DNA repair. We further evaluated the impact of amino acid substitutions using the Polyphen2 prediction program; we focused in particular on the T448M missense mutation of RNF8, which is an E3-ligase polyubiquitylating γ-H2AX. The T448M mutation was close to the RING domain (Fig. 7a). To assess the ubiquitylation status of γ-H2AX, we examined X-ray-irradiated TE-6 and TE-1 cells by Western blotting (Fig. 7b). In the TE-1 cells, the levels of mono- and di-ubiquitinated γ-H2AX were increased at 2 h after irradiation and decreased at 6 h after irradiation. Meanwhile, no significant increase in ubiquitination was observed in the TE-6 cells (Fig. 7b–d).

Discussion

To date, the anti-tumor effects of PARP inhibitors to ESCC have not been evaluated both *in vitro* and *in vivo*. In this study, we identified TE-6 cells as AZD2281-sensitive cell line for the first time. The following findings support the idea that the PARP inhibitor induced growth retardation in the DSB repair-impaired background of TE-6 cells: (i) AZD2281 induced the accumulation of DNA damage, as evaluated by γ-H2AX expression levels. (ii) AZD2281 induced the accumulation of a tetraploid cell population in a time-dependent manner, consistent with previous reports that cells with accumulated unrepaired DSBs caused in every S-phase are arrested at G2/M boundary.[27] (iii) Sustained damage to DNA, the attenuated ubiquitination of γ-H2AX and a defect in DSB repair nuclear foci formation under X-ray irradiation suggest that TE-6 cells have an impaired DNA repair ability.

Several genomic biomarkers that predict the efficacy of PARP inhibitors have been identified. Though the presence or absence of *BRCA1* and *BRCA2* alterations most strikingly distinguishes the PARP inhibitor-sensitive cells and patients, no pathogenetic mutations in either gene were identified in the TE-6 cells (Table S1). Consistent with this, expression of BRCA1 and BRCA 2 proteins were not reduced in TE-6 cells (Fig. S3a,b). The alteration of other genes, such as *53BP1*, *RAD51*, *PTEN* and *USP11*, also reportedly affects the sensitivity to PARP inhibitors.[18,28–32] To identify the genomic events corresponding to the AZD2281 sensitivity of TE-6 cells, we performed whole-exome sequencing. Because a paired non-tumor genome is not available for the TE-series cells, we subtracted previously identified germline variants from our set of total SNVs and indels to enrich for potential somatic mutations. Among the remaining mutations, we focused on those located in the genes encoding DNA repair-related proteins and identified a novel mutation of *RNF8*. RNF8 is an E3-ligase

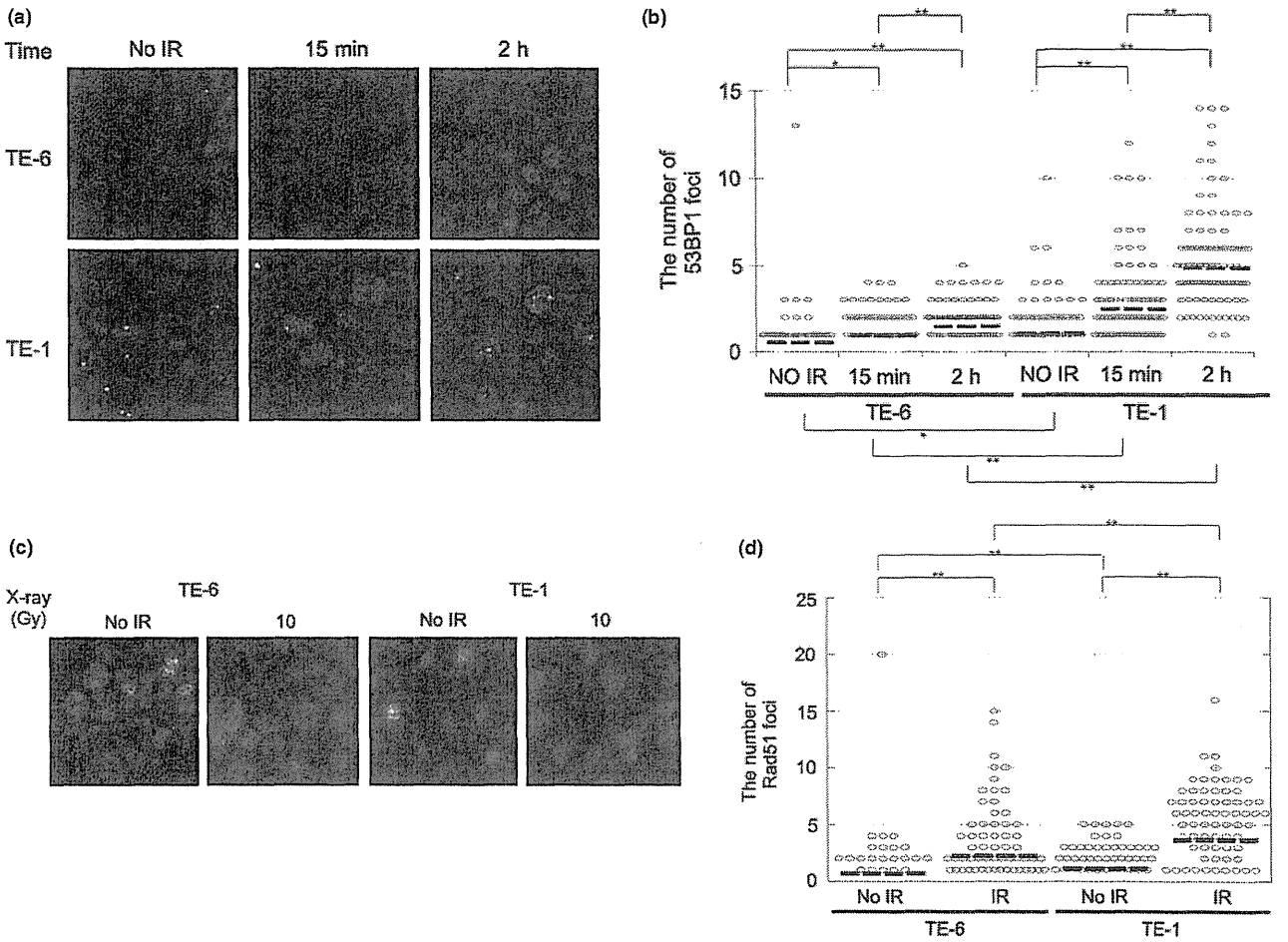

Fig. 6. Impairment of 53BP1 and RAD51 nuclear focus formation in X-ray irradiated TE-6 cells. (a) TE-6 and TE-1 cells were irradiated with 2 Gy of X-rays and fixed 15 min and 2 h after irradiation. The formation of 53BP1 nuclear foci was evaluated by immunofluorescence. (b) Scatter diagrams showing the number of 53BP1 foci in individual cells. The lines shown indicate the mean of the data plotted. The data were obtained from at least 100 cells for each condition. $*P < 0.05$, $**P < 0.01$ (Student's *t*-test). (c) TE-6 and TE-1 cells were irradiated with 10 Gy of X-rays and fixed 6 h after irradiation. The formation of RAD51 nuclear foci was evaluated by immunofluorescence. (d) Scatter diagrams showing the number of RAD51 foci in individual cells. The lines shown indicate the mean of the data plotted. The data were obtained from at least 100 cells for each condition. $**P < 0.01$ (Student's *t*-test).

Table 3. Mutations in the DNA repair-related genes uniquely identified in the exome of TE-6 cells

Novel mutations of DNA repair involved genes of TE-6

Gene	Chr.	Position	Base change	Variant frequency (%)	Amino acid alteration	PolyPhen2 prediction
RNF8	6	37349032	C>T	100	T448M	Probably damaging
CHAF1A	19	4429530	G>A	87	R567Q	Probably damaging
CEP164	11	117222670	A>G	88.9	D120G	Probably damaging
CLSPN	1	36217027	C>T	19.4	A618T	Benign
POLK	5	74865291	A>G	55	I128V	Benign
ATRX	X	76952184	G>A	100	S84L	Benign

targeting γ-H2AX that accumulates at DNA DSBs and recruits repair proteins, including 53BP1 and RAD51.[33–35] It was reported that *RNF8*$^{-/-}$ *p53*$^{-/-}$ mice had increased levels of genomic instability and a remarkably elevated tumor incidence compared to *p53*$^{-/-}$ mice,[36] that the knockdown of RNF8 sensitized cells to ionizing radiation, and that disruption of the RING domains of RNF8 impaired DSB-associated ubiquitylation and inhibited retention of 53BP1 and BRCA1 at the DSBs sites.[33] The PolyPhen-2 program predicts a probable deleterious impact of the T448M substitution on the structure and function of RNF8. Although the effect of the T448M mutation on the polyubiquitination ability of RNF8 has not yet been confirmed, the observation that the increase in ubiquitination after X-ray irradiation in the TE-6 cells was less than that of the TE-1 cells suggests that RNF8 is impaired in the TE-6 cells. We hypothesized that this mutation might affect the polyubiquitination ability of RNF8 and, as a result, contribute to the DSB repair defect to some extent. The impact of the mutation or loss of RNF8 to PARP inhibitor sensitivity has to be further evaluated.

Whether RNF8 is the only factor contributing to TE-6 sensitivity should be carefully considered. The anti-tumor effect of PARP inhibitors is obviously determined by the BRCA1 or BRCA2 status in ovarian and breast cancers.[37] Meanwhile, the sensitivity of the TE-series cells to AZD2281 is altered by

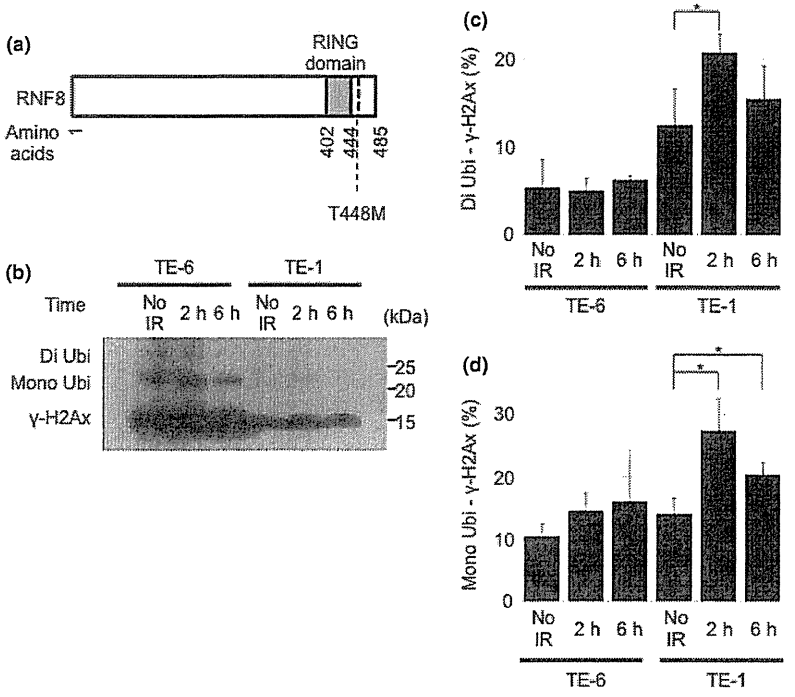

Fig. 7. A novel mutation in the RNF8 gene and the reduced ability of TE-6 cells to polyubiquitinate γ-H2AX. (a) The structure of RNF8 protein and a newly identified T448M amino acid-substitution mutation. (b) Western blot analysis of γ-H2Ax in TE-6 and TE-1 cells treated with 2 Gy of X-rays. (c) The proportion of diubiquitinated γ-H2Ax standardized to non-ubiquitinated γ-H2Ax. The data represent the averages and standard deviations of three independent experiments. (d) The proportion of monoubiquitinated γ-H2Ax standardized to non-ubiquitinated γ-H2Ax. The data represent the averages and standard deviations of three independent experiments.

gradation and most cells exhibited intermediate sensitivity. It may suggest that the AZD2281 sensitivity was regulated by multiple molecular mechanisms in each cell line rather than a single molecule. This multiplicity might make it difficult to identify the distinctive genomic biomarkers of PARP inhibitor sensitivity in ESCC.

We noticed a strong correlation between AZD2281 sensitivity and γ-H2Ax levels in the cells without treatment; this effect might represent the extent of baseline DNA damage. Double strand breaks regularly occur in proliferating cells because topoisomerases bind to DNA and cut the phosphate backbone of the DNA during DNA replication. Though these DSBs are properly repaired in non-tumor cells, it is plausible that unrepaired DNA remains in tumor cells with impaired DSB repair, such as the TE-6 cells. Once a correlation between the baseline level of γ-H2Ax expression and DSB repair defect is further confirmed, the amount of γ-H2Ax in a tumor tissue sample could be a reasonable biomarker for selecting preferable patients for PARP inhibitor therapy. Further clinical and biological studies of this effect are warranted.

Acknowledgments

The authors thank Dr Hiroko Onozuka for helpful discussions and technical support. This work was supported by the National Cancer Center Research and Development Fund (23-A-8, 15) and a grant for the Third Term Comprehensive 10-year Strategy for Cancer Control from the Ministry of Health, Labour and Welfare (H22-033).

Disclosure Statement

The authors have no conflict of interest.

References

1 Jemal A, Bray F, Center MM, Ferlay J, Ward E, Forman D. Global cancer statistics. *CA Cancer J Clin* 2011; **61**: 69–90.
2 Jamieson GG, Mathew G, Ludemann R, Wayman J, Myers JC, Devitt PG. Postoperative mortality following oesophagectomy and problems in reporting its rate. *Br J Surg* 2004; **91**: 943–7.
3 Müller JM, Erasmi H, Stelzner M, Zieren U, Pichlmaier H. Surgical therapy of oesophageal carcinoma. *Br J Surg* 1990; **77**: 845–57.
4 Zhang X, Watson DI, Jamieson GG, Lally C, Bessell JR, Devitt PG. Outcome of oesophagectomy for adenocarcinoma of the oesophagus and oesophagogastric junction. *ANZ J Surg* 2005; **75**: 513–9.
5 Crumley AB, Going JJ, McEwan K *et al.* Endoscopic mucosal resection for gastroesophageal cancer in a U.K. population. Long-term follow-up of a consecutive series. *Surg Endosc* 2011; **25**: 543–8.
6 Lewis JJ, Rubenstein JH, Singal AG, Elmunzer BJ, Kwon RS, Piraka CR. Factors associated with esophageal stricture formation after endoscopic mucosal resection for neoplastic Barrett's esophagus. *Gastrointest Endosc* 2011; **74**: 753–60.
7 Fujishiro M, Yahagi N, Kakushima N *et al.* Endoscopic submucosal dissection of esophageal squamous cell neoplasms. *Clin Gastroenterol Hepatol* 2006; **4**: 688–94.
8 Herskovic A, Martz K, al-Sarraf M *et al.* Combined chemotherapy and radiotherapy compared with radiotherapy alone in patients with cancer of the esophagus. *N Engl J Med* 1992; **326**: 1593–8.
9 al-Sarraf M, Martz K, Herskovic A *et al.* Progress report of combined chemoradiotherapy versus radiotherapy alone in patients with esophageal cancer: an intergroup study. *J Clin Oncol* 1997; **15**: 277–84.
10 Ame JC, Spenlehauer C, de Murcia G. The PARP superfamily. *BioEssays* 2004; **26**: 882–93.
11 Gallmeier E, Kern SE. Absence of specific cell killing of the BRCA2-deficient human cancer cell line CAPAN1 by poly(ADP-ribose) polymerase inhibition. *Cancer Biol Ther* 2005; **4**: 703–6.
12 Bryant HE, Schultz N, Thomas HD *et al.* Specific killing of BRCA2-deficient tumours with inhibitors of poly(ADP-ribose) polymerase. *Nature* 2005; **434**: 913–7.
13 Venkitaraman AR. Cancer susceptibility and the functions of BRCA1 and BRCA2. *Cell* 2002; **108**: 171–82.

14 Weston VJ, Oldreive CE, Skowronska A *et al.* The PARP inhibitor olaparib induces significant killing of ATM-deficient lymphoid tumor cells in vitro and in vivo. *Blood* 2010; **116**: 4578–87.
15 Williamson CT, Muzik H, Turhan AG *et al.* ATM deficiency sensitizes mantle cell lymphoma cells to poly(ADP-ribose) polymerase-1 inhibitors. *Mol Cancer Ther* 2010; **9**: 347–57.
16 Dedes KJ, Wetterskog D, Mendes-Pereira AM *et al.* PTEN deficiency in endometrioid endometrial adenocarcinomas predicts sensitivity to PARP inhibitors. *Sci Transl Med* 2010; **2**: 53–75.
17 McEllin B, Camacho CV, Mukherjee B *et al.* PTEN loss compromises homologous recombination repair in astrocytes: implications for glioblastoma therapy with temozolomide or poly(ADP-ribose) polymerase inhibitors. *Cancer Res* 2010; **70**: 5457–64.
18 Wiltshire TD, Lovejoy CA, Wang T, Xia F, O'Connor MJ, Cortez D. Sensitivity to poly(ADP-ribose) polymerase (PARP) inhibition identifies ubiquitin-specific peptidase 11 (USP11) as a regulator of DNA double-strand break repair. *J Biol Chem* 2010; **285**: 14565–71.
19 Akbari MR, Malekzadeh R, Lepage P *et al.* Mutations in Fanconi anemia genes and the risk of esophageal cancer. *Hum Genet* 2011; **129**: 573–82.
20 Rosenberg PS, Alter BP, Ebell W. Cancer risks in Fanconi anemia: findings from the German Fanconi Anemia Registry. *Haematologica* 2008; **93**: 511–7.
21 Stransky N, Egloff AM, Tward AD *et al.* The mutational landscape of head and neck squamous cell carcinoma. *Science* 2011; **333**: 1157–60.
22 Drew Y, Mulligan EA, Vong WT *et al.* Therapeutic potential of poly(ADP-ribose) polymerase inhibitor AG014699 in human cancers with mutated or methylated BRCA1 or BRCA2. *J Natl Cancer Inst* 2011; **103**: 334–46.
23 Sakai W, Swisher EM, Karlan BY *et al.* Secondary mutations as a mechanism of cisplatin resistance in BRCA2-mutated cancers. *Nature* 2008; **451**: 1116–20.
24 Rodrigue A, Lafrance M, Gauthier MC *et al.* Interplay between human DNA repair proteins at a unique double-strand break in vivo. *EMBO J* 2006; **25**: 222–31.
25 Mochan TA, Venere M, DiTullio RA Jr, Halazonetis TD. 53BP1, an activator of ATM in response to DNA damage. *DNA Repair (Amst)* 2004; **3**: 945–52.
26 Baumann P, West SC. Role of the human RAD51 protein in homologous recombination and double-stranded-break repair. *Trends Biochem Sci* 1998; **23**: 247–51.
27 Farmer H, McCabe N, Lord CJ *et al.* Targeting the DNA repair defect in BRCA mutant cells as a therapeutic strategy. *Nature* 2005; **434**: 917–21.
28 Bunting SF, Callén E, Wong N *et al.* 53BP1 inhibits homologous recombination in Brca1-deficient cells by blocking resection of DNA breaks. *Cell* 2010; **141**: 243–54.
29 McCabe N, Turner NC, Lord CJ *et al.* Deficiency in the repair of DNA damage by homologous recombination and sensitivity to poly(ADP-ribose) polymerase inhibition. *Cancer Res* 2006; **66**: 8109–15.
30 Mendes-Pereira AM, Martin SA, Brough R *et al.* Synthetic lethal targeting of PTEN mutant cells with PARP inhibitors. *EMBO Mol Med* 2009; **1**: 315–22.
31 Turner NC, Ashworth A. Biomarkers of PARP inhibitor sensitivity. *Breast Cancer Res Treat* 2011; **127**: 283–6.
32 Wang X, Weaver DT. The ups and downs of DNA repair biomarkers for PARP inhibitor therapies. *Am J Cancer Res* 2011; **1**: 301–27.
33 Mailand N, Bekker-Jensen S, Faustrup H *et al.* RNF8 ubiquitylates histones at DNA double-strand breaks and promotes assembly of repair proteins. *Cell* 2007; **131**: 887–900.
34 Bekker-Jensen S, Mailand N. Assembly and function of DNA double-strand break repair foci in mammalian cells. *DNA Repair (Amst)* 2010; **9**: 1219–28.
35 Lu CS, Truong LN, Aslanian A *et al.* The RING finger protein RNF8 ubiquitinates Nbs1 to promote DNA double-strand break repair by homologous recombination. *J Biol Chem* 2012; **287**: 43984–94.
36 Halaby MJ, Hakem A, Li L *et al.* Synergistic interaction of Rnf8 and p53 in the protection against genomic instability and tumorigenesis. *PLoS Genet* 2013; **9**: e1003259.
37 Fong PC, Boss DS, Yap TA *et al.* Inhibition of poly(ADP-ribose) polymerase in tumors from BRCA mutation carriers. *N Engl J Med* 2009; **361**: 123–34.

Supporting Information

Additional supporting information may be found in the online version of this article:

Data S1. Materials and methods.

Fig. S1. Effect of AZD2281 on the colony formation of TE-8, TE-10, TE-4, TE-11, TE-14, TE-9 and HCC1937 cells.

Fig. S2. Effect of BSI-201 on the colony formation of TE-1 and TE-6 cells.

Fig. S3. DNA ploidy of TE-1 andTE-6 cells treated with AZD2281 for 12 h.

Fig. S4. Expression of the BRCA1 and BRCA2 proteins in TE-series cells.

Fig. S5. Expression of the 53BP1 and RAD51 proteins in TE-1 and TE-6 cells.

Table S1. Summary of the whole exome sequencing data of TE-1 cells.

Table S2. Summary of the whole exome sequencing data of TE-6 cells.

NPC Natural Product Communications

2014
Vol. 9
No. 1
79 - 82

Antiausterity Activity of Arctigenin Enantiomers: Importance of (2*R*,3*R*)-Absolute Configuration

Suresh Awale[a], Mamoru Kato[b], Dya Fita Dibwe[b], Feng Li[b], Chika Miyoshi[c], Hiroyasu Esumi[c], Shigetoshi Kadota[b] and Yasuhiro Tezuka[b,*]

[a]*Frontier Research Core for Life Sciences, University of Toyama, 2630 Sugitani, Toyama 930-0194, Japan*

[b]*Institute of Natural Medicine, University of Toyama, Sugitani-2630, Toyama 930-0194, Japan*

[c]*Cancer Physiology Project, Research Center for Innovative Oncology, National Cancer Center Hospital East, Chiba, Japan*

tezuka@inm.u-toyama.ac.jp

Received: August 30th, 2013; Accepted: September 24th, 2013

From a MeOH extract of powdered roots of *Wikstroemia indica*, six dibenzyl-γ-butyrolactone-type lignans with (2*S*,3*S*)-absolute configuration [(+)-arctigenin (**1**), (+)-matairesinol (**2**), (+)-trachelogenin (**3**), (+)-nortrachelogenin (**4**), (+)-hinokinin (**5**), and (+)-kusunokinin (**6**)] were isolated, whereas three dibenzyl-γ-butyrolactone-type lignans with (2*R*,3*R*)-absolute configuration [(−)-arctigenin (**1***), (−)-matairesinol (**2***), (−)-trachelogenin (**3***)] were isolated from *Trachelospermum asiaticum*. The *in vitro* preferential cytotoxic activity of the nine compounds was evaluated against human pancreatic PANC-1 cancer cells in nutrient-deprived medium (NDM), but none of the six lignans (**1**–**6**) with (2*S*,3*S*)-absolute configuration showed preferential cytotoxicity. On the other hand, three lignans (**1***–**3***) with (2*R*,3*R*)-absolute configuration exhibited preferential cytotoxicity in a concentration-dependent manner with PC_{50} values of 0.54, 6.82, and 5.85 μM, respectively. Furthermore, the effect of (−)- and (+)-arctigenin was evaluated against the activation of Akt, which is a key process in the tolerance to nutrition starvation. Interestingly, only (−)-arctigenin (**1***) strongly suppressed the activation of Akt. These results indicate that the (2*R*,3*R*)-absolute configuration of (−)-enantiomers should be required for the preferential cytotoxicity through the inhibition of Akt activation.

Keywords: Preferential cytotoxicity, *Wikstroemia indica*, Human pancreatic PANC-1 cell line, (2*R*,3*R*)-Absolute configuration.

Pancreatic cancer is the most aggressive form of cancer and has an exceptionally high global mortality rate, with an estimated 267,000 deaths worldwide in 2008. It ranks 8th or 9th as the most frequent cause of cancer death worldwide and is the 4th or 5th most frequent cause of cancer death in most developed countries, including the United States, Europe, and Japan. Moreover, it has been estimated that the number of deaths from pancreatic cancer will reach 484,000 by 2030 [1]. As cancers increase in size, their immediate environment often becomes heterogeneous and some regions of large cancers often possess microenvironmental niches, which exhibit a significant gradient of critical metabolites including oxygen, glucose, other nutrients, and growth factors [2]. Thus, angiogenesis is regarded as the key step in tumor progression, and antiangiogenesis is the most promising cancer therapy, and extensive studies have been conducted to prevent tumor angiogenesis. However, pancreatic cancer survives with an extremely poor blood supply and becomes more malignant [3]. It is also largely resistant to most known chemotherapeutic agents, including 5-fluorouracil, Taxol®, doxorubicin, cisplatin, and camptothecin [4]. Therefore, effective chemotherapeutic agents that target pancreatic cancer are urgently needed. Human pancreatic cancer cells show a remarkable tolerance to extreme nutrient starvation [5], enabling them to survive under hypovascular conditions. Therefore, it has been hypothesized that eliminating the tolerance of cancer cells to nutrition starvation may allow a novel biochemical approach, known as "anti-austerity", for cancer therapy [6,7]. Considering this hypothesis, we searched for anti-austerity agents in medicinal plants using the human pancreatic cancer cell line PANC-1 and identified (−)-arctigenin as an active constituent of *Arctium lappa* [8].

In a continuing study, we examined the preferential cytotoxicity of arctigenin-related compounds and the following structural moieties could be concluded to be important for the preferential cytotoxicity of arctigenin: 1) the 3-hydroxy-4-methoxyphenyl group at the 2-position on the γ-butyrolactone ring, 2) the less polar substituent at the 3-position on the γ-butyrolactone ring, and 3) the γ-butyrolactone ring [9]. On the other hand, it is well known that the chirality is important for pharmacological activity and/or toxicity [10,11]. In order to clarify the effect of the absolute configuration, we examined the preferential cytotoxicity of (+)-arctigenin derivatives.

(+)-Arctigenin derivatives are reported to be contained in *Wikstroemia indica* C.A.Mey (Thymelaeaceae) [10]. Thus, a dry $CHCl_3$ extract from powdered roots of *W. indica* was separated by MPLC, followed by purification by preparative TLC, to give six (+)-enantiomers of arctigenin (**1**) [10], matairesinol (**2**) [13], trachelogenin (**3**) [14], nortrachelogenin (**4**) [15], hinokinin (**5**) [16], and kusunokinin (**6**) [13], which have the 2*S*,3*S* absolute configuration (Figure 1). In the separation procedure, we also obtained a new guaian-type sesquiterpene (4,10,11-guaiatrien-3-one-14-oic acid) and eight known compounds: oleodaphnal, 1α,7α,10α*H*-guaia-4,11-dien-3-one, 7-methoxycoumarin, 7-hydroxycoumarin (umbelliferone), daphnogitin, daphnoretin, salicifoliol, and (−)-pinoresinol [17].

Among the seven arctigenin derivatives, on the other hand, (−)-enantiomers of arctigenin (**1***) [9], matairesinol (**2***) [9], and trachelogenin (**3***) [18] were isolated from a $CHCl_3$ extract of the powdered stems of *Trachelospermum asiaticum* Nakai (Apocynaceae).

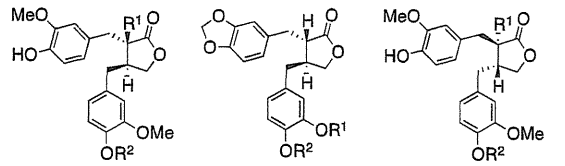

Figure 1: Dibenzyl-γ-butyrolactone-type lignans isolated from *W. indica* (**1**–**6**) and *T. asiaticum* (**1***–**3***).

Then, we evaluated the *in vitro* preferential cytotoxic activity of all of the isolated compounds against human pancreatic cancer PANC-1 cells in nutrient-deprived medium (NDM) (Figure 2). The PANC-1 cell line is highly resistant to nutrient starvation, and can survive in NDM even after 48 h of starvation [6–8]. This tolerance to nutrient starvation was reported to be eliminated by (–)-arctigenin and (–)-matairesinol [8,9]. As reported, (–)-enantiomers [(–)-arctigenin (**1***), (–)-matairesinol (**2***), and (–)-trachelogenin (**3***)], which have the (2*R*,3*R*)-absolute configuration, exhibited preferential cytotoxicity in a concentration-dependent manner with PC_{50} values of 0.54, 6.82, and 5.85 μM, respectively. However, the corresponding (+)-enantiomers [(+)-arctigenin (**1**), (+)-matairesinol (**2**), and (+)-trachelogenin (**3**)], which have the (2*S*,3*S*)-absolute configuration, showed no cytotoxicity both in NDM and in nutrient-rich medium (DMEM). Likewise, other (+)-enantiomers [(+)-nortrachelogenin (**4**), (+)-hinokinin (**5**), and (+)-kusunokinin (**6**)] having the 2*S*,3*S* absolute configuration also exhibited no cytotoxicity. Thus, the (2*R*,3*R*)-absolute configuration of (–)-enantiomers should be important for the preferential cytotoxicity. Likewise, none of the other isolated constituents revealed preferential cytotoxicity.

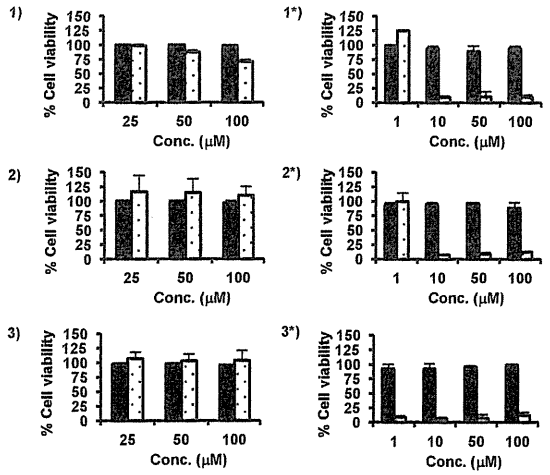

Figure 2: Effects of both enantiomers of arctigenin, matairesinol, and trachelogenin on cell survival in the PANC-1 cell line under either DMEM (■) or NDM (□) condition. Data, mean from triplicate experiments. The cell number at the start of the starvation was considered to be 100%. The numbers **1**–**3** and **1***–**3*** mean the compound number.

We then performed Western blot analysis to see the effect of a (+)- and (–)-arctigenin against the activation of protein kinase B (PKB)/Akt, a key pathway involved in the cell survival mechanism in an austerity environment [5–7].

The serine/threonine kinase PKB/Akt is constitutively activated in a majority of human pancreatic cancer cell lines [19]. High

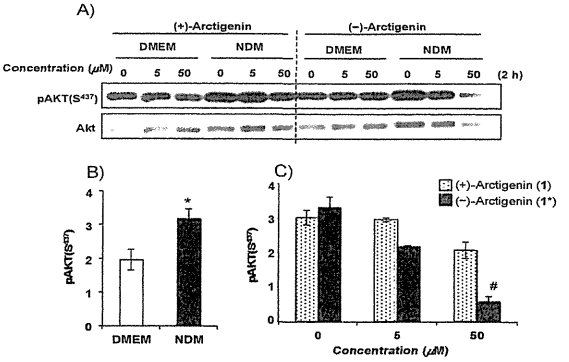

Figure 3: Effect of arctigenin enantiomers against the activation of Akt in DMEM and NDM conditions. A) Representative Western blot showing phospho-Akt (Ser437) and total Akt. B) Phospho-Akt (Ser437) expression in DMEM and NDM conditions. C) Concentration dependent inhibition of phospho-Akt (Ser437) by the enantiomers of arctigenin in NDM. Data represent the mean of three Western blot experiments. Signal intensities (pixel × 10^4) were calculated using ImageJ software (NIH). *,#: significantly different ($p < 0.01$) from either DMEM or control in NDM, respectively.

expression of phospho-Akt (Ser437) has been observed in PANC-1 cells exposed to nutrient starvation conditions, which is associated with the tolerance to nutrient deprivation, hypoxic, and other stress states [5]. Therefore, increased phospho-Akt (Ser437) expression is one of the austerity markers, and its inhibition is in part responsible for their preferential cytotoxicity during nutrient deprivation by antiausterity agents [8]. Therefore, we examined the effect of both (+)- and (–)-arctigenin enantiomers against the activation of Akt in DMEM and in NDM. As shown in Figure 3, there was an approximately 1.5-fold increment of phospho-Akt (Ser437) in PANC-1 cells in NDM compared with PANC-1 cells in DMEM at 120 min of exposure. However, this effect was significantly diminished by (–)-arctigenin (**1***) in a concentration-dependent manner. On the other hand, the effect of (+)-arctigenin (**1**) was too weak. These results clearly suggest that inhibition of Akt activation by (–)-arctigenin (**1***) is responsible for the preferential death of PANC-1 cells in NDM. (+)-Arctigenin (**1**), which showed a weak inhibition of phospho-Akt (Ser437) expression, exhibited only a weak preferential cytotoxicity in NDM. These results strongly support the strict requirement of the (2*R*,3*R*)-absolute configuration in (–)-arctigenin (**1***) and its derivative for the preferential cytotoxicity through the inhibition of Akt activation.

Experimental

General: Optical rotations were recorded on a JASCO DIP-140 digital polarimeter. IR spectra were measured with a Shimadzu IR-408 spectrophotometer in $CHCl_3$ solution. NMR spectra were recorded on a JEOL JNM-LA400 spectrometer with tetramethylsilane (TMS) as internal standard. HR-EI-MS were obtained on a JEOL JMS-700T mass spectrometer. Medium-pressure liquid chromatography (MPLC) was performed with a Büchi pump module C-650 system. CC was performed with silica gel (60N, spherical, neutral, 40–50 μm, Kanto Chemical Co., Inc.) or reversed-phase silica gel (Cosmosil $75C_{18}$-OPN, Nakalai Tesque, Inc.). Analytical and preparative TLC was conducted on either precoated silica gel $60F_{254}$ or RP-$18F_{254}$ plates (Merck, 0.25 or 0.50 mm thickness).

Plant material: Roots of *Wikstroemia indica* C.A.Mey (Thymelaeaceae) (Lot. No. 090401) were purchased from Anhui Wansheng Chinese Traditional Medicine Electuary Co., Ltd., Anhui, China in April, 2009. Stems of *Trachelospermum asiaticum* Nakai (Apocynaceae) were collected at Toyama, Japan on February,

2009 and authenticated by Mr Hiroharu Fujino (Faculty of Pharmaceutical Sciences, University of Toyama).

***Isolation procedure from* Wikstroemia indica:** The powdered roots of *W. indica* (1 kg) were extracted with MeOH (3 × 6 L, 1 h each) under sonication; the mixture was filtered and the filtrate evaporated under reduced pressure to give the MeOH extract (76.4 g). Part of this (25 g) was separated by MPLC on a silica gel column (40–50 μm, 3 × 15 cm, precolumn 3 × 7 cm, flow rate 20 mL/min) eluted using a step gradient of MeOH–$CHCl_3$ and the eluates were combined to 6 fractions based on their behavior on TLC (fr. 1: 5% MeOH–$CHCl_3$, 730 mg; fr. 2: 10% MeOH–$CHCl_3$, 430 mg; fr. 3: 15% MeOH–$CHCl_3$, 1.54 g; fr. 4: 20% MeOH–$CHCl_3$, 1.99 g; fr. 5: 25% MeOH–$CHCl_3$, 1.71 g; fr. 6: 30% MeOH–$CHCl_3$, 2.64 g). Fraction 2 was separated by reversed-phase preparative TLC with 50% MeOH–H_2O to give **5** [16] (2.2 mg), oleodaphnal [20] (2.3 mg), and daphnoretin [21,22] (46.9 mg). Fraction 3 was separated by reversed-phase preparative TLC with 30% MeOH–H_2O to give **2** [13] (3.6 mg), **6** [13] (6.2 mg), 1α,7α,10α*H*-guaia-4,11-dien-3-one [23] (8.1 mg), 7-methoxycoumarin [24] (3.0 mg), daphnogitin [21,25] (17.8 mg), salicifoliol [26] (5.1 mg), and (−)-pinoresinol [27,28] (4.5 mg). Fraction 4 was separated by reversed-phase preparative TLC with 30% MeOH–H_2O to give **1** (3.3 mg), **3** (8.6 mg), **4** (437 mg), 4,10,11-guaiatrien-3-one-14-oic acid [17] (2.5 mg), and 7-hydroxycoumarin (umbelliferone) [29,21] (2.9 mg).

Isolation procedure from* Trachelospermum asiaticum:** The powdered stems of *T. asiaticum* (3.1 kg) were extracted with $CHCl_3$ (2 × 10 L, 1 h each) under sonication; the mixture was filtered and the filtrate evaporated under reduced pressure to give a $CHCl_3$ extract (73.6 g). Part of this (12.5 g) was separated by CC on silica gel with a AcOEt: *n*-hexane solvent system and the eluates were combined to 13 fractions based on their behavior on TLC (fr. 1: 20% AcOEt–*n*-hexane, 99.6 mg; fr. 2: 25% AcOEt–*n*-hexane, 594 mg; fr. 3: 45% AcOEt–*n*-hexane, 1.66 g; fr. 4: 50% AcOEt–*n*-hexane, 193 mg; fr. 5: 60% AcOEt–*n*-hexane, 341 mg; fr. 6: 65% AcOEt–*n*-hexane, 215 mg; fr. 7: 70% AcOEt–*n*-hexane, 180 mg; fr. 8: 75% AcOEt–*n*-hexane, 240 mg; fr. 9: 80% AcOEt–*n*-hexane, 237 mg; fr. 10: 85% AcOEt–*n*-hexane, 300 mg; fr. 11: 90% AcOEt–*n*-hexane, 212 mg; fr. 12: 95% AcOEt–*n*-hexane, 830 mg; fr. 13: AcOEt eluate, 191 mg). Fraction 12 was separated by preparative TLC with 5% acetone–$CHCl_3$ to give **1 [9] (24.6 mg), **2*** [9] (6.5 mg), and **3*** [18] (22.5 mg).

Cells and culture: Human pancreatic cancer PANC-1 cell line was maintained in Dulbecco's modified Eagle's medium (DMEM, Nissui Pharmaceutical Co., Ltd.) supplemented with 10% fetal bovine serum (FBS, Gibco BRL Products, Gaithersburg, MD, USA), and 1% antibiotic–antimycotic solution (Sigma–Aldrich Inc.). Nutrient deprived medium (NDM) contained 265 mg/L $CaCl_2 \cdot 2H_2O$, 0.1 mg/L $Fe(NO_3) \cdot 9H_2O$, 400 mg/L KCl, 200 mg/L $MgSO_4 \cdot 7H_2O$, 6400 mg/L NaCl, 700 mg/L $NaHCO_3$, 125 mg/L NaH_2PO_4, 15 mg/L phenol red, 1 M HEPES buffer (pH 7.4, Wako Pure Chemical Industries, Ltd., Osaka, Japan), and 10 mL MEM vitamin solution (Life Technologies, Inc., Rockville, MD, USA). The final pH was adjusted to 7.4 with 10% $NaHCO_3$. For amino acid supplementation, stock solutions (200 mM L-glutamine solution, MEM amino acids solution, and MEM nonessential amino acids solution; Life Technologies) were added at a concentration of 1%.

Preferential cytotoxicity: Preferential cytotoxicity was determined as previously described [8]. In brief, PANC-1 cells (2×10^4 cells/well) were seeded in 96-well plates (Corning Inc., Corning, NY, USA) and incubated in fresh DMEM at 37°C under 5% CO_2 and 95% air for 24 h. The cells were washed with Dulbecco's phosphate-buffered saline (PBS, Nissui Pharmaceutical Co., Ltd., Tokyo, Japan) before the medium was replaced with either DMEM or NDM containing serial dilutions of the test samples. After 24 h of incubation, the cells were washed with PBS, and 100 μL of DMEM containing 10% WST-8 cell counting kit solution (Dojindo, Kumamoto, Japan) was added to the wells. After 3 h of incubation, the absorbance was measured at 450 nm. Cell viability was calculated from the mean values for 3 wells using the following equation: Cell viability (%) = $[(Abs_{(test\ samples)} - Abs_{(blank)})/(Abs_{(control)} - Abs_{(blank)})] \times 100$. The preferential cytotoxicity was expressed as the concentration at which 50% of cells died preferentially in NDM (PC_{50}).

Western blot analysis: The proteins were separated by gel electrophoresis on a polyacrylamide gel containing 0.1% SDS and then transferred to nitrocellulose membranes. The membranes were blocked with PBS containing 5%, w/v, skim milk, washed with PBS containing 0.3% Tween 20 (Sigma), then incubated overnight at room temperature with Akt antibody and the phosphospecific (Ser437) Akt antibody (New England Biolabs, Ipswich, MA) diluted with PBS. After washing, the membranes were incubated for 2 h at room temperature with horseradish peroxidase-conjugated goat anti-rabbit IgG (Santa Cruz Biotechnology, Santa Cruz, CA) as the second antibody. The bands were detected with an enhanced chemiluminescence system (Amersham Biosciences UK Ltd., Buckinghamshire, United Kingdom). Quantitative analysis of Western blot was carried out with ImageJ software (NIH).

Acknowledgments - This work was supported in part by grants from the Ministry of Health and Welfare for the Third Term Comprehensive 10 Year Strategy for Cancer Control and by MEXT/JSPS KAKENHI Grant Number 22590098.

References

[1] Ferlay J, Shin HR, Bray F, Forman D, Mathers C, Parkin DM. (**2010**) GLOBOCAN 2008 v1.2, Cancer Incidence and Mortality Worldwide: IARC CancerBase No. 10 [Internet]. Lyon, France: International Agency for Research on Cancer. http://globocan.iarc.fr, accessed on 28/08/2013.

[2] Dang CV, Semenza GL. (**1999**) Oncogenic alteration of metabolism. *Trends in Biochemical Sciences*, ***24***, 68–72.

[3] Kitano M, Kudo M, Maekawa K, Suetomi Y, Sakamoto H, Fukuta N, Nakaoka R, Kawasaki T. (**2004**) Dynamic imaging of pancreatic diseases by contrast enhanced coded phase inversion harmonic ultrasonography. *Gut*, ***53***, 854–859.

[4] Chung HW, Bang SM, Park SW, Chung JB, Kang JK, Kim JW, Seong JS, Lee WJ, Song SY. (**2004**) A prospective randomized study of gemcitabine with doxifluridine versus pacritaxel with doxifluridine in concurrent chemoradiotherapy for locally advanced pancreatic cancer. *International Journal of Radiation Oncology, Biology, Physics*, ***60***, 1494–1501.

[5] Izuishi K, Kato K, Ogura T, Kinoshita T, Esumi H. (**2000**) Remarkable tolerance of tumor cells to nutrient deprivation: possible new biochemical target for cancer therapy. *Cancer Research*, ***60***, 6201–6207.

[6] Esumi H, Lu J, Kurashima Y, Hanaoka T. (**2004**) Antitumor activity of pyrvinium pamoate, 6-(dimethylamino)-2-[2-(2,5-dimethyl-1-phenyl-1*H*-pyrrol-3-yl)ethenyl]-1-methyl-quinolinium pamoate salt, showing preferential cytotoxicity during glucose starvation. *Cancer Science*, ***95***, 685–690.

[7] Lu J, Kunimoto S, Yamazaki Y, Kaminishi M, Esumi H. (**2004**) Kigamicin D, a novel anticancer agent based on a new anti-austerity strategy targeting cancer cells' tolerance to nutrient starvation. *Cancer Science*, ***95***, 547–552.

[8] Awale S, Lu J, Kalauni SK, Kurashima Y, Tezuka Y, Kadota S, Esumi H. (**2006**) Identification of arctigenin as an antitumor agent having the ability to eliminate the tolerance of cancer cells to nutrient starvation. *Cancer Research*, ***66***, 1751–1757.
[9] Tezuka Y, Yamamoto K, Awale S, Li F, Yomoda S, Kadota S. (**2013**) Anti-austeric activity of phenolic constituents of seeds of *Arctium lappa*. *Natural Product Communications*, ***8***, 463–466.
[10] Suzuki H, Lee KH, Haruna M, Iida T, Ito K, Huang HC. (**1982**) (+)-Arctigenin, a lignan from *Wikstroemia indica*. *Phytochemistry*, ***21***, 1824–1825.
[11] Kuling K, Nowicki P, Malawska B. (**2004**) Influence of the absolute configuration on pharmacological activity of antihypertensive and antiarrythmic drugs. *Polish Journal of Pharmacology*, ***56***, 499–508.
[12] Islam MR, Mahdi JG, Bowen ID. (**1997**) Pharmacological importance of stereochemical resolution of enantiomeric drugs. *Drug Safety*, ***17***, 149–165.
[13] Okunishi T, Umezawa T, Shimada M. (**2000**) Enantiomeric compositions and biosynthesis of *Wikstroemia sikokiana* lignans. *Journal of Wood Science*, ***46***, 234–242.
[14] Moritani Y, Fukushima C, Ukita T, Miyagishima T, Ohmizu H, Iwasaki T. (**1996**) Stereoselective syntheses of *cis*- and *trans*-isomers of α-hydroxy-α,β-dibenzyl-γ-butyrolactone lignans: new syntheses of (±)-trachelogenin and (±)-guayadequiol. *Journal of Organic Chem*istry, ***61***, 6922–6930.
[15] Wang L-Y, Uehara N, Kitanaka S. (**2005**) Lignans from the roots of *Wikstroemia indica* and their DPPH radical scavenging and nitric oxide inhibitory activities. *Chemical & Pharmaceutical Bulletin*, ***53***, 1348–1351.
[16] Lin R-W, Tsai I-L, Duh C-Y, Lee K-H, Chen I-S. (**2004**) New lignans and cytotoxic constituents from *Wikstroemia lanceolata*. *Planta Medica*, ***70***, 234–238.
[17] Kato M, He Y-M, Li F, Awale S, Kadota S, Tezuka Y. (**2014**) New guaian-type sesquiterpene from *Wikstroemia indica*. *Natural Product Communications*, ***9***, 1-2.
[18] John LMD, Tinto WF. (**1992**) Revised ^{13}C-nmr assignments for the biologically active butyrolactone (–)-trachelogenin. *Journal of Natural Products*, ***55***, 1313–1314.
[19] Vivanco I, Sawyers CL. (**2002**) The phosphatidylinositol 3-kinase–AKT pathway in human cancer. *Nature Reviews Cancer*, ***2***, 489–501.
[20] Taninaka H, Takaishi Y, Honda G, Imakura Y, Sezik E, Yesilada E. (**1999**) Terpenoids and aromatic compounds from *Daphne oleoides* ssp. *oleoides*. *Phytochemistry*, ***52***, 1525–1529.
[21] Yao H, Zhong Y, Yin J. (**2007**) Chemical components of *Wikstroemia indica* C.A. Meyer. *Zhongcaoyao*, ***38***, 669–670.
[22] Chakrabarth R, Das B, Banerji J. (**1986**) *Bis*-coumarins from *Edgeworthia gardneri*. *Phytochemistry*, ***25***, 557–558.
[23] Lin R-W, Tsai I-L, Duh C-Y, Lee K-H, Chen I-S. (**2004**) New lignans and cytotoxic constituents from *Wikstroemia lanceolata*. *Planta Medica*, ***70***, 234–238.
[24] Osborne AG. (**1989**) ^{13}C NMR spectral studies of some methoxycoumarin derivatives. A re-assignment for citropten (limettin) and an examination of *peri*-proximity effects for the methyl-methoxy and methoxy-methyl couples. *Magnetic Resonance in Chemistry*, ***27***, 348–354.
[25] Liao S-G, Zhang B-L, Wu Y, Yue J-M. (**2005**) New phenolic components from *Daphne giraldii*. *Helvetica Chimica Acta*, ***88***, 2873–2878.
[26] González AG, Estévez-Reyes R, Mato C. (**1989**) Salicifoliol, a new furolactone-type lignan from *Bupleurum salicifolium*. *Journal of Natural Products*, ***52***, 1139–1142.
[27] Zhuang L, Seligmann O, Jurcic K, Wagner H. (**1982**) Constituents of *Daphne tangutica*. *Planta Medica*, ***45***, 172–176.
[28] Carpinella MC, Giorda LM, Ferrayoli CG, Palacios SM. (**2003**) Antifungal effects of different organic extracts from *Melia azedarach* L. on phytopathogenic fungi and their isolated active components. *Journal of Agricultural & Food Chemistry*, ***51***, 2506–2511.
[29] Wijeratne EMK, Bandara BMR, Gunatilaka AAL, Tezuka Y, Kikuchi T. (**1992**) Chemical constituents of three Rutaceae species from Sri Lanka. *Journal of Natural Products*, ***55***, 1261–1269.

Arctigenin Inhibits Osteoclast Differentiation and Function by Suppressing Both Calcineurin-Dependent and Osteoblastic Cell-Dependent NFATc1 Pathways

Teruhito Yamashita[1]*, Shunsuke Uehara[2], Nobuyuki Udagawa[2], Feng Li[3], Shigetoshi Kadota[3], Hiroyasu Esumi[4], Yasuhiro Kobayashi[1], Naoyuki Takahashi[1]

1 Institute for Oral Science, Matsumoto Dental University, Shiojiri, Nagano, Japan, **2** Department of Biochemistry, Matsumoto Dental University, Shiojiri, Nagano, Japan, **3** Institute of Natural Medicine, University of Toyama, Toyama, Japan, **4** National Cancer Center Hospital East, Kashiwa, Chiba, Japan

Abstract

Arctigenin, a lignan-derived compound, is a constituent of the seeds of *Arctium lappa*. Arctigenin was previously shown to inhibit osteoclastogenesis; however, this inhibitory mechanism has yet to be elucidated. Here, we showed that arctigenin inhibited the action of nuclear factor of activated T-cells, cytoplasmic 1 (NFATc1), a key transcription factor for osteoclastogenesis. NFATc1 in osteoclast precursors was activated through two distinct pathways: the calcineurin-dependent and osteoblastic cell-dependent pathways. Among the several lignan-derived compounds examined, arctigenin most strongly inhibited receptor activator of nuclear factor κB ligand (RANKL)-induced osteoclast-like cell formation in mouse bone marrow macrophage (BMM) cultures, in which the calcineurin-dependent NFATc1 pathway was activated. Arctigenin suppressed neither the activation of nuclear factor κB and mitogen-activated protein kinases nor the up-regulation of c-Fos expression in BMMs treated with RANKL. However, arctigenin suppressed RANKL-induced NFATc1 expression. Interestingly, the treatment of osteoclast-like cells with arctigenin converted NFATc1 into a lower molecular weight species, which was translocated into the nucleus even in the absence of RANKL. Nevertheless, arctigenin as well as cyclosporin A (CsA), a calcineurin inhibitor, suppressed the NFAT-luciferase reporter activity induced by ionomycin and phorbol 12-myristate 13-acetate in BMMs. Chromatin immunoprecipitation analysis confirmed that arctigenin inhibited the recruitment of NFATc1 to the promoter region of the NFATc1 target gene. Arctigenin, but not CsA suppressed osteoclast-like cell formation in co-cultures of osteoblastic cells and bone marrow cells, in which the osteoblastic cell-dependent NFATc1 pathway was activated. The forced expression of constitutively active NFATc1 rescued osteoclastogenesis in BMM cultures treated with CsA, but not that treated with arctigenin. Arctigenin also suppressed the pit-forming activity of osteoclast-like cells cultured on dentin slices. These results suggest that arctigenin induces a dominant negative species of NFATc1, which inhibits osteoclast differentiation and function by suppressing both calcineurin-dependent and osteoblastic cell-dependent NFATc1 pathways.

Citation: Yamashita T, Uehara S, Udagawa N, Li F, Kadota S, et al. (2014) Arctigenin Inhibits Osteoclast Differentiation and Function by Suppressing Both Calcineurin-Dependent and Osteoblastic Cell-Dependent NFATc1 Pathways. PLoS ONE 9(1): e85878. doi:10.1371/journal.pone.0085878

Editor: João Costa-Rodrigues, Faculdade de Medicina Dentária, Universidade do Porto, Portugal

Received September 6, 2013; **Accepted** December 3, 2013; **Published** January 17, 2014

Funding: This work was supported by Grants-in-Aid for Scientific Research (24592821, 21592378 and 22390351) from the Japan Society for the Promotion of Science (http://www.jsps.go.jp/). The funder had no role in study design, data collection and analysis, decision to publish, or preparation of the manuscript.

Competing Interests: The authors have declared that no competing interests exist.

* E-mail: teru@po.mdu.ac.jp

Introduction

Arctigenin, a lignan-derived compound, is one of the constituents of the seeds of *Arctium lappa*. Arctigenin is a biologically active lignan with anti-tumor, anti-inflammatory, anti-oxidant, anti-proliferative, and anti-diabetic activities. Arctigenin was shown to block the activation of Akt signaling induced by glucose starvation in pancreatic tumors [1,2]. Arctigenin also exhibited anti-inflammatory properties against lipopolysaccharide in a macrophage cell line by suppressing inducible nitric oxide synthase expression and mitogen-activated protein (MAP) kinase signals [3,4]. Arctigenin was recently shown to inhibit osteoclast formation in mouse bone marrow macrophage (BMM) cultures [5]. However, the precise mechanism by which arctigenin inhibits osteoclast development remains to be determined.

Osteoclasts are bone-resorbing multinucleated cells formed from monocyte/macrophage-lineage precursors [6,7]. Osteoblastic cells such as immature osteoblast-lineage cells, osteoblasts, and osteocytes regulate the differentiation of osteoclast precursors into osteoclasts. Osteoblastic cells express two cytokines that are responsible for osteoclastogenesis: macrophage colony-stimulating factor (M-CSF, also called colony-stimulating factor 1) and receptor activator of nuclear factor κB ligand (RANKL) [8–12]. Osteoclast precursors have been shown to express c-Fms (the receptor of M-CSF) and RANK (the receptor of RANKL) and differentiate into osteoclasts in the presence of M-CSF and RANKL [13,14]. Osteoblastic cells also express osteoprotegerin (OPG), a decoy receptor of RANKL. OPG inhibits osteoclast differentiation by suppressing the interaction between RANKL and RANK. Osteoclasts also express RANK, and the RANKL-RANK interaction was shown to induce the bone-resorbing activity of osteoclasts [6,7].

A previous study showed that bone-resorption stimulating factors such as 1α,25-dihydroxyvitamin D_3 [1α,25$(OH)_2D_3$],

parathyroid hormone, and prostaglandin E_2 (PGE_2) enhanced the expression of RANKL in osteoblastic cells [7]. RANKL activates RANK-mediated signaling, including MAP kinases, nuclear factor κB (NF-κB), c-Fos, and nuclear factor of activated T-cells, cytoplasmic 1 (NFATc1). These RANK-mediated signals induce the expression of osteoclast-related genes such as tartrate-resistant acid phosphatase (TRAP, coded by *Acp5*), cathepsin K (*Ctsk*), osteoclast-associated receptor (*Oscar*), and *Nfatc1* itself [15–17].

NFATc1 was identified as a key transcription factor for osteoclastogenesis [15,18]. The Ca^{2+} oscillation/calcineurin-dependent activation and amplification of NFATc1 in osteoclast precursors are essential for their differentiation into osteoclasts. RANKL induces Ca^{2+} oscillations in osteoclast precursors, and these oscillations activate calcineurin, a Ca^{2+}-dependent phosphatase. Activated calcineurin then dephosphorylates multiple serine residues in the NFATc1 protein, which permits the nuclear translocation of NFATc1. NFATc1 in the nucleus acts as a transcription factor for genes specifically expressed in osteoclasts such as *Acp5*, *Ctsk*, *Oscar*, and *Nfatc1* itself. The calcineurin inhibitors, cyclosporin A (CsA) and FK506, have been shown to suppress RANKL-induced osteoclast formation in BMM cultures.

Osteoclastogenesis induced by RANKL also requires co-stimulatory receptor signaling through adaptors containing immunoreceptor tyrosine-based activation motifs (ITAMs). ITAM-containing proteins, such as DNAX-activating protein 12 (DAP12) and Fc receptor common γ chain (FcRγ), facilitate the calcium-mobilizing mechanism during osteoclastogenesis [19–22]. Thus, RANK and ITAM signalings cooperated to induce calcium oscillations, resulting in the activation of NFATc1. FcRγ and DAP12 are adaptor molecules that associate with immunoglobulin-like receptors such as OSCAR, triggering receptor expressed on myeloid cells 2 (TREM2), signal-regulatory protein β1 (SIRPβ1) and paired immunoglobulin-like receptor A (PIR-A). OSCAR and PIR-A use FcRγ, while TREM2 and SIRPβ1 associate with DAP12. Recently, Barrow *et al.* reported that OSCAR bound to a specific motif of collagen and stimulated osteoclastogenesis [23]. These results suggest that osteoblastic cells express not only RANKL and M-CSF but also ligands for immunoglobulin-like receptors.

Besides Ca^{2+}/calcineurin-dependent signaling, the osteoblastic cell-dependent pathway has also been shown to activate NFATc1 [24,25]. BMMs obtained from type 2 inositol-1,2,5-triphosphate receptor (IP_3R2) knockout mice exhibited neither RANKL-induced Ca^{2+} oscillations nor RANKL-induced differentiation into osteoclasts. However, IP_3R2-deficient osteoclast precursors could normally differentiate into osteoclasts when they were co-cultured with osteoblastic cells. This Ca^{2+} oscillation-independent osteoclastogenesis was shown to be insensitive to FK506 [24]. Kuroda *et al.* recently showed that Cot, a serine/threonine kinase, was involved in the activation and amplification of NFATc1 in the absence of Ca^{2+} oscillations. Cot in osteoclast precursors was activated by cell-cell interactions with osteoblastic cells. Activated Cot increased NFATc1 protein levels through phosphorylation-dependent protein stabilization, thereby amplifying NFATc1 [25]. Cot likely phosphorylates residues of NFATc1 that differ from those targeted by calcineurin-mediated dephosphorylation. Although the osteoblastic cell-derived molecules that activate Cot in osteoclast precursors is unknown, Cot-mediated NFATc1 stabilization contributes to osteoclastogenesis *in vivo*. Mice doubly deficient in DAP12 and FcRγ exhibited severe osteopetrosis owing to the lack of osteoclasts [22]. These results suggest that both calcineurin-dependent and osteoblastic cell-dependent activations of NFATc1 are physiologically important in controlling osteoclast differentiation *in vivo*.

The aim of this study was to elucidate the inhibitory mechanism of arctigenin on the osteoclast differentiation and function. Especially, we examined the intracellular signals including NFATc1 in detail. Arctigenin converted NFATc1 into a lower molecular species, which was translocated in the nucleus of osteoclast-like cells even in the absence of RANKL. Arctigenin inhibited osteoclast-like cell formation not only in BMM cultures, but also in co-cultures of osteoblastic cells and bone marrow cells. In addition, arctigenin suppressed the pit-forming activity of osteoclast-like cells cultured on dentin. These results suggest that arctigenin suppresses both calcineurin-dependent and osteoblastic cell-dependent NFATc1 pathways through the generation of a dominant species of NFATc1.

Materials and Methods

Reagents and animals

Arctigenin, arctiin, and secoisolariciresinol were purified from *Arctium lappa* and single peaks were confirmed by high performance liquid chromatography. The chemical structures of these compounds were shown in Figure 1A. Human recombinant RANKL was purchased from PeproTech (Rocky Hill, NJ). Human M-CSF (Leukoprol) was obtained from Kyowa Hakko (Tokyo, Japan). $1\alpha,25(OH)_2D_3$ was from Wako Pure Chemical (Osaka, Japan). CsA, PGE_2, phorbol 12-myristate 13-acetate (PMA), and ionomycin were from Calbiochem-Sigma (St. Louis, MO). Antibodies for p38, ERK, JNK, IκBα, AKT, and NF-κB p65, and antibodies for phosphorylated forms of p38, ERK, JNK, IκBα, and AKT were from Cell Signaling Technology (Danvers, MA). Antibodies for NFATc1 (7A6), Lamin A/C, and β-actin were obtained from Thermo (Rockford, IL), Santa Cruz (Dallas, TX), and Sigma, respectively. Other chemicals used were of analytical grade. Newborn and 6-week-old ddY mice were purchased from Japan SLC (Shizuoka, Japan).

Ethics statement

All animal experiments in this study were approved by the Institutional Animal Care and Use Committee of Matsumoto Dental University. All steps were performed to limit suffering in all animal experiments.

In vitro osteoclast-like cell differentiation

Mouse BMMs were prepared as previously described [26]. Briefly, mouse bone marrow cells were cultured for 16 h in α-modified minimal essential medium (α-MEM) with 10% fetal bovine serum (FBS) and 5000 U/mL M-CSF. Non-adherent cells were then collected and used as BMMs. BMMs (3×10^4 cells/well) for osteoclast formation assay were cultured for 3 days in 96-well culture plates in the presence of 5000 U/mL M-CSF and 100 ng/mL RANKL together with increasing concentrations of lignan-derived compounds or 0.1% dimethyl sulfoxide (DMSO, vehicle control). Osteoblastic cells were obtained form newborn mouse calvariae for the co-culture experiments. Bone marrow cells (1×10^5 cells/well) and calvarial osteoblastic cells (1×10^4 cells/well) were co-cultured for 6 days in α-MEM with 10% FBS in the presence of 10 nM $1\alpha,25(OH)_2D_3$ together with or without test compounds. After cultivation for the indicated periods, cells were fixed and stained for TRAP. TRAP-positive multinucleated cells containing more than three nuclei were counted as osteoclast-like cells. The effects of lignan-derived compounds on the proliferation of BMMs were also evaluated. BMMs (1×10^3 cells/well) were cultured with increasing concentrations of lignan-derived compounds in 96-well culture plates. The cultures were subjected to the cell viability Alamar Blue assay (Invitrogen, Carlsbad, CA).

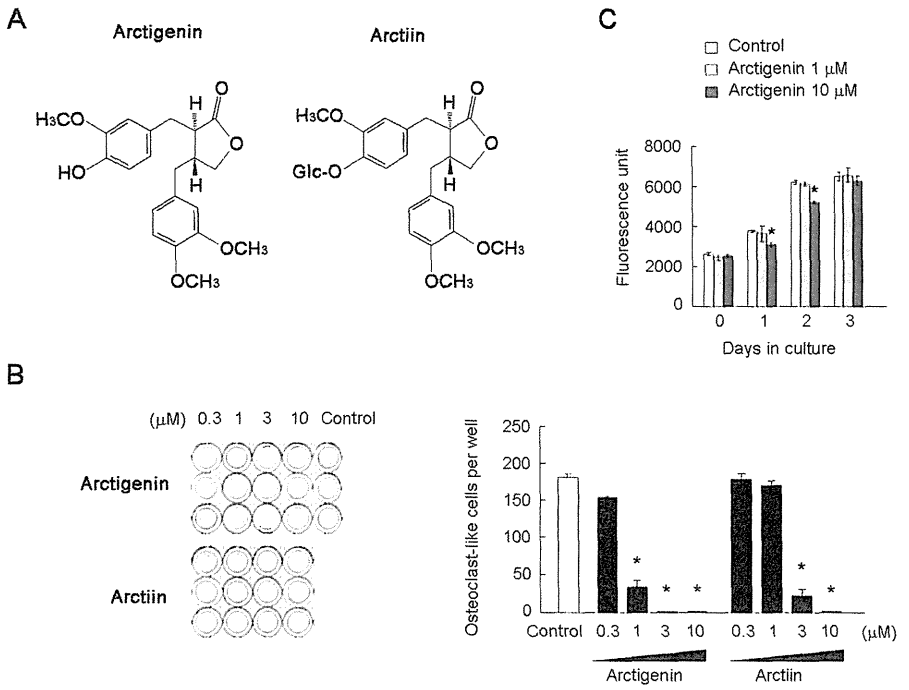

Figure 1. Effects of arctigenin on osteoclast-like cell formation and cell proliferation in BMM cultures. (A) Chemical structures of arctigenin, arctiin, and secoisolariciresinol. (B) Effects of lignan-derived compounds on osteoclast-like cell formation in BMM cultures. BMMs were cultured in 96-well culture plates in the presence of RANKL and M-CSF together with increasing concentrations of the lignan-derived compounds. After cultivation for 3 days, cells were stained for TRAP. TRAP-positive cells appeared as dark red cells. TRAP-positive multinucleated cells containing more than three nuclei were counted as osteoclast-like cells. (C) Effects of arctigenin on the proliferation of BMMs. BMMs were cultured in the presence of M-CSF together with increasing concentrations of arctigenin. Cell proliferation was evaluated on days 0, 1, 2, and 3 using an Alamar Blue assay. The results were expressed as means +/− SD (n = 3). *, $p<0.05$.
doi:10.1371/journal.pone.0085878.g001

Pit formation assay and actin ring staining

Functionally active osteoclast-like cells were prepared using a mouse co-culture system [27]. Bone marrow cells (1×10^7 cells) and osteoblastic cells (1×10^6 cells) were co-cultured in collagen gel-coated 10-cm plates in the presence of 10 nM $1\alpha,25(OH)_2D_3$ and 1 μM PGE_2. After a co-culture for 7 days, the collagen-gel plate was treated with collagenase. All cells recovered were suspended in 10 mL of α-MEM containing 10% FBS, and were used as osteoclast-like cell preparations. Osteoclast-like cell preparations were plated on dentin slices (a square piece of 4 mm, 0.75 mm in thickness) in 96-well culture plates (0.2 mL/well) and incubated for 1 h. Dentin slices were then transferred into 48-well culture plates and cultured for an additional 48 h in α-MEM containing 10% FBS (0.5 mL/well) together with or without 1 μM arctigenin. Dentin slices were then recovered, fixed, and stained for TRAP. TRAP-positive cells were counted as osteoclast-like cells. Cells on the slices were removed by cotton swabs and slices were further stained with Mayer's hematoxylin to detect resorbing pits. Resorption pit areas were measured using ImageJ software. To evaluate actin ring formation by osteoclast-like cells, cells on dentin slices were fixed, permeabilized with 0.2% Triton X-100/PBS, and stained with rhodamine-phalloidin (Invitrogen).

Western blot analysis

Cells were lysed in lysis buffer [20 mM Tris-HCl, pH7.6, 150 mM NaCl, 1 mM EDTA, 50 mM β-glycerophosphate, 1% NP-40, and supplemented with 1× protease inhibitor cocktail (Sigma)], sonicated, and supernatants were collected as total cell lysates. Lysates (20 μg/lane) were electrophoresed on SDS-PAGE gels, transferred to polyvinylidene difluoride membranes, and subjected to immunoblotting using the ECL plus chemiluminescence detection system (GE Healthcare, Buckinghamshire, UK).

RNA isolation and quantitative RT-PCR

Total RNA was isolated using TRIzol reagent (Invitrogen). Reverse transcription was performed on 1 μg of RNA using oligo(dT) primers and ReverTra Ace reverse transcriptase (Toyobo Life Science, Osaka). cDNA was then amplified using SYBR green Taq RT-PCR reagent (Takara Bio, Shiga, Japan) and expression levels were quantified using the Opticon II real-time PCR instrument (Bio-Rad, Hercules, CA). The primers used for PCR were as follows; *Gapdh*: 5′-TGT GTC CGT CGT GGA TCT GA-3′ (forward) and 5′-TTG CTG TTG AAG TCG CAG GAG-3′ (reverse); *Nfatc1*: 5′-TGG AGA AGC AGA GCA CAG AC-3′ (forward) and 5′-GCG GAA AGG TGG TAT CTC AA-3′ (reverse); *c-Fos*: 5′-CCG AGC TGG TGC ATT ACA GAG A-3′ (forward) and 5′-TGG ATG CTT GCA AGT CCT TGA G-3′ (reverse); *Acp5*: 5′-TTG CGA CCA TTG TTA GCC ACA TA-3′ (forward) and 5′-TCA GAT CCA TAG TGA AAC CGC AAG-3′ (reverse); *Ctsk*: 5′-CAG CAG AAC GGA GGC ATT GA-3′ (forward) and 5′-CTT TGC CGT GGC GTT ATA CAT ACA-3′ (reverse); *Oscar*: 5′-CGT GCT GAC TTC ACA CCA ACA-3′ (forward) and 5′-CAC AGC GCA GGC TTA CGT T-3′ (reverse); *Rankl*: 5′-CAT GTG CCA CTG AGA ACC TTG AA-3′ (forward) and 5′ CAG GTC CCA GCG CAA TGT AAC-3′ (reverse); *Opg*: 5′-CAT GAG GTT CCT GCA CAG CTT C-3′

(forward) and 5′-ACA GCC CAG TGA CCA TTC CTA GTT A-3′ (reverse); *IL-2*: 5′-GCT GTT GAT GGA CCT ACA GGA-3′ (forward) and 5′-TTC AAT TCT GTG GCC TGC TT-3′ (reverse); *GM-CSF*: 5′-GCA TGT AGA GGC CAT CAA AGA-3′ (forward) and 5′ CGG GTC TGC ACA CAT GTT A-3′ (reverse).

Nuclear extract preparation

Crude osteoclast-like cell preparations were cultured for 4 h on 24-well culture plates. Osteoblastic cells were then removed by washing with 0.1% trypsin/EDTA solution. Purified osteoclast-like cells were further cultured with M-CSF for 16 h. Cells were then incubated for 20 min with 1 μM arctigenin, 1 μg/mL CsA, or 0.1% DMSO (vehicle control) in the presence or absence of 100 ng/mL RANKL. Nuclear and cytoplasmic fractions were prepared using a nuclear extraction kit (Active Motif, Carlsbad, CA) and subjected to Western blot analysis.

Immunocytochemical localization of NFATc1

The localization of NFATc1 was immunocytochemically examined [28]. Purified osteoclast-like cells on glass coverslips were further cultured for 16 h in the presence of M-CSF, but in the absence of RANKL. Osteoclast-like cells were then incubated for 20 min with 1 μM arctigenin, 100 ng/mL RANKL, or 0.1% DMSO (vehicle control). Cells were fixed with 4% paraformaldehyde, permeabilized with 0.2% Triton X-100/PBS, and blocked with 2% BSA/PBS. An anti-NFATc1 antibody was added to cell preparations, followed by incubation with biotinylated goat anti-mouse IgG and fluorescein-conjugated streptavidin (Vector Laboratories, Burlingame, CA). Nuclei were counterstained with propidium iodide (PI).

Forced expression of NFATc1

BMMs were retrovirally transduced with NFATc1 cDNA. The constitutively active (ca)-NFATc1 mutant with the alanine substitution of twenty serine residues, which are typically phosphorylated, was shown to be autonomously translocated into the nucleus [29]. The pCX4pur-ca-NFATc1 (constitutively active), pCX4pur-wt-NFATc1 (wild-type), or pCX4pur-GFP control plasmid was transfected into the retrovirus packaging cell line Plat-E [30]. BMMs were incubated for 2 days with virus-rich supernatant in the presence of M-CSF and polybrene. Infected BMMs were further cultured for 3 days with M-CSF and RANKL. Nuclear and cytoplasmic fractions were prepared from infected BMMs as described above, and subjected to Western blot analysis.

Luciferase reporter assay

The luciferase reporter plasmid pNFAT-Luc, which contained four copies of the NFAT binding site, 5′-GGA GGA AAA ACT GTT TCA TAC AGA AGG CGT-3′, was used (Stratagene-Agilent, La Jolla, CA). BMMs were transfected by electroporation in serum-free solution with Nucleofector II (Amaxa Biosystems-Lonza, Basel, Switzerland). Forty-eight hours after transfection, cells were stimulated with 1 μM ionomycin and 20 nM PMA, in the presence or absence of arctigenin and CsA. Cells were lysed 24 h after stimulation, and luciferase activity was measured with a luciferase assay system (Promega, Madison, WI).

Chromatin immunoprecipitation (ChIP) assay

BMMs were stimulated with M-CSF and RANKL for 2 days to form mononuclear pre-osteoclast-like cells. These cells were further treated with 100 ng/mL RANKL in the presence or absence of 1 μM arctigenin. Cells were crosslinked with 1% formaldehyde 1 h after the treatment and a nuclear fraction was extracted. The protein-chromatin complex was immunoprecipitated overnight at 4°C with the anti-NFATc1 antibody or control IgG after shearing DNA by sonication. Fragmented DNA were purified and amplified by PCR using primers specific for the *Oscar* promoter [17]: 5′-GAA CAC CAG AGG CTA TGA CTG TTC-3′ and 5′-CCG TGG AGC TGA GGA AAA GGT TG-3′.

Cultures of osteoblastic cells

Osteoblastic cells were obtained from newborn mouse calvariae as described [27]. Osteoblastic cells were cultured in α-MEM with 10% FBS. Osteoblastic cells were cultured in the presence or absence of 10 nM $1\alpha,25(OH)_2D_3$ together with or without 1 μM arctigenin for gene expression analysis. The expression of *Rankl* and *Opg* mRNAs was analyzed after cultivation for 24 h by quantitative RT-PCR. Osteoblastic cells were cultured in the presence or absence of 1 μM arctigenin to stain for alkaline phosphatase, a marker of osteoblasts. After cultivation for 6 days, cells were fixed and stained for alkaline phosphatase. Osteoblastic cells were cultured with increasing concentrations of arctigenin for the cell growth assay. The cultures were then subjected to the cell viability Alamar Blue assay (Invitrogen).

Statistical analysis

All data were expressed as the mean +/− SD. Differences were evaluated by Mann-Whitney's U-test. P values less than 0.05 were considered to be significant. All experiments were independently repeated at least three times and similar results were obtained.

Results

Effect of lignan-derived compounds on osteoclast-like cell formation

Arctigenin, arctiin, and secoisolariciresinol are major lignan-derived compounds of *Arctium lappa*. We first compared the inhibitory effects of these compounds on osteoclast-like cell formation in mouse BMM cultures (Fig. 1 and Fig. S1). Mouse BMMs were cultured in the presence of RANKL and M-CSF together with increasing concentrations of these compounds. Osteoclast-like cells formed within 3 days in control cultures. Arctigenin and arctiin inhibited osteoclast-like cell formation in a dose-dependent manner (Fig. 1B). Arctigenin showed stronger inhibitory effects on osteoclast-like cell formation than that of arctiin. Secoisolariciresinol failed to inhibit osteoclast-like cell formation (Fig. S1). Thus, arctigenin showed the strongest inhibitory effect on osteoclast-like cell formation among the three lignans. We next examined the effects of arctigenin on the growth of BMMs (Fig. 1C). Arctigenin had little effect on the growth of BMMs, through 10 μM arctigenin slightly suppressed it on days 1 and 2. The treatment of BMMs with granulocyte-macrophage colony-stimulating factor (GM-CSF) induced their differentiation into dendritic cells. Arctigenin at 1 μM had no inhibitory effect on the dendritic differentiation of BMMs (Fig. S2).These results suggested that the inhibitory effect of arctigenin was specific for osteoclast-like cell differentiation, and was not due to its action on cell growth. Arctigenin at 1 μM inhibited osteoclast-like cell formation more strongly than arctiin did. Therefore, arctigenin at 1 μM was used in further experiments.

Effect of arctigenin on RANKL-induced signaling in osteoclastogenesis

RANKL was previously shown to induce the transcription of osteoclast-related genes such as *Acp5*, *Ctsk*, and *Oscar* by activating NFATc1 [15]. The expression of *Nfatc1* itself was also shown to be up-regulated during osteoclastogenesis [31]. We examined the effect of arctigenin on the expression of these osteoclast-related genes in BMMs during osteoclastogenesis (Fig. 2A). Arctigenin reduced the expression of *Acp5*, *Ctsk*, and *Oscar* at each time point. The expression of the transcription factors, *Nfatc1* and *c-Fos*, was also up-regulated by the treatment with RANKL. The RANKL-induced up-regulation of *Nfatc1* expression, but not that of *c-Fos*, was reduced by arctigenin throughout the experimental period.

We next examined the effect of arctigenin on RANKL-induced signals in BMMs (Fig. 2B). RANKL has been shown to activate NF-κB and MAP kinases, including p38 MAP kinase, ERK, and JNK [32,33]. Western blot analysis revealed that these signals were similarly activated by RANKL in BMMs in the presence and absence of 1 μM arctigenin (Fig. 2B). A previous study showed that Akt was one of the targets of arctigenin in tumor cells. The phosphorylation of Akt in BMMs was up-regulated by RANKL, and arctigenin had little effect on this phosphorylation (Fig. 2B). These results suggested that arctigenin inhibited other pathways involved in osteoclastogenesis, independent of MAP kinase, NF-κB, and c-Fos signaling.

We next compared the inhibitory action of arctigenin with that of the well-known inhibitors of osteoclastogenesis, CsA (a calcineurin-NFAT inhibitor) and SB203580 (a p38 MAP kinase inhibitor). Arctigenin, CsA, and SB203580 were added to BMM cultures at different time points (Fig. 2C). Osteoclast-like cell formation was inhibited by the addition of these agents during the entire culture period (0-3 days). Arctigenin and CsA, but not SB203580 inhibited osteoclast-like cell formation when they were added 24 h after RANKL stimulation (1–3 days). Thus, signals mediated by p38 MAP kinase appeared to be necessary for the commitment of osteoclast precursors but not for the expression of osteoclast-related markers in the committed cells [34]. The inhibitory action of arctigenin on osteoclastogenesis was similar to that of CsA. These results suggested that NFATc1 was a target molecule of the arctigenin action in BMMs.

Effects of arctigenin on the transcriptional activity and localization of NFATc1 in osteoclast-like cells

Osteoclast-like cells, which were formed in BMM cultures in the presence of RANKL for 3 days, highly expressed NFATc1 (Fig. 2A). Using purified osteoclast-like cells obtained from co-cultures performed in collagen gel-coated plates, we examined the effect of arctigenin on the nuclear localization of NFATc1 (Fig. 3A). Osteoclast-like cells were cultured overnight in RANKL-free medium. Cells were then treated with RANKL together with or without arctigenin and CsA. Interestingly, NFATc1 was translocated into the nuclei of osteoclast-like cells in response to arctigenin even in the absence of RANKL (Fig. 3A, lane 3). CsA did not show such activity, and inhibited the nuclear translocation of NFATc1 induced by RANKL in osteoclast-like cells (Fig. 3A, lanes 5 and 6). NF-κB p65 was also translocated into the nuclei of osteoclast-like cells in response to RANKL (Fig. 3A, lanes 2, 4, and 6). Neither arctigenin nor CsA inhibited the nuclear translocation of NF-κB p65 (Fig. 3A, lanes 4 and 6). Immunocytochemical analysis confirmed that arctigenin, even in the absence of RANKL, promoted the nuclear localization of NFATc1 in osteoclast-like cells (Fig. 3B). The nuclear localization of NFATc1 was also observed in osteoclast-like cells treated with RANKL.

Treating cells with ionomycin and PMA led to Ca^{2+} oscillations, which induced the nuclear translocation of NFATc1 through the activation of calcineurin. We then examined the effect of arctigenin on the transcriptional activity of NFATc1 in BMMs using a luciferase reporter assay, in which the luciferase gene was driven by the NFAT-binding site (Fig. 3C). The treatment of BMMs with ionomycin and PMA increased NFAT-driven luciferase activity in BMM cultures. Arctigenin as well as CsA suppressed the luciferase activity enhanced by ionomycin and PMA. We then examined whether arctigenin inhibited the recruitment of NFATc1 on the target gene promoters by using a ChIP assay with the *Oscar* promoter (Fig. 3D). BMMs treated with RANKL for 2 days were further cultured in the presence or absence of arctigenin. RANKL stimulation induced the recruitment of NFATc1 on the *Oscar* promoter (Fig. 3D, lane 3), whereas arctigenin inhibited it (Fig. 3D, lane 4). These results indicated that arctigenin inhibited NFATc1 transcriptional activity by suppressing the recruitment of NFATc1 onto the target gene promoter, and also that the mechanism for the inhibitory action of arctigenin on osteoclast formation was different from that of CsA.

NFATc1 is commonly retained in the cytosol as a multi-phosphorylated form. Ca^{2+} oscillations activate calcineurin, which dephosphorylates NFATc1 [29,30]. We examined the effect of arctigenin on the molecular mass of NFATc1 in osteoclast-like cells (Fig. 3E). NFATc1 in osteoclasts was recognized as a broad band around 90 kDa (Fig. 3E, lane 1). In contrast, NFATc1 in osteoclast-like cells treated with arctigenin was detected as a major band at 85 kDa (Fig. 3E, lane 3). NFATc1 in osteoclast-like cells treated with CsA accumulated as a band at approximately 100 kDa, which may have been due to the hyper-phosphorylation of NFATc1. It was reported that calf intestine alkaline phosphatase (CIAP) dephosphorylated NFATc1 at more than 20 phosphorylated amino acid residues and produced lower molecular weight species of NFATc1 *in vitro* [37]. NFATc1 in these cell lysates shifted to approximately 85 kDa after being treated with CIAP (Fig. 3E, lanes 2 and 4). These results suggest that arctigenin converted NFATc1 into a lower molecular weight species.

Effect of arctigenin on osteoclastogenesis induced by the forced expression of NFATc1

The constitutively active NFATc1 mutant (ca-NFATc1) was shown to be autonomously translocated into the nucleus [37]. We examined whether the forced expression of ca-NFATc1 could rescue arctigenin-inhibited osteoclastogenesis (Fig. 4). BMMs were retrovirally transduced with ca-NFATc1, wild-type (wt)-NFATc1, and control GFP cDNA. The forced expression of ca-NFATc1, but not wt-NFATc1 in BMMs rescued osteoclast-like cell formation inhibited by CsA (Fig. 4A, lowest panels). In contrast, ca-NFATc1 failed to rescue osteoclastogenesis inhibited by arctigenin. Western blot analysis confirmed that ca-NFATc1 was mainly located in the nucleus of BMMs, whereas wt-NFATc1 was dominantly retained in the cytosol (Fig. 4B). These results suggest that arctigenin did not inhibit the nuclear translocation of ca-NFATc1, but reduced its transcriptional activity. It was also reported that the survival of thymocytes was supported by interleukin 7 (IL-7) through the phosphorylation of Tyr-371 in NFATc1, and the forced expression of Y371F-NFATc1 mutant enhanced the thymocyte survival [38]. Therefore, we examined the effect of the Y371F mutant of NFATc1 on osteoclastogenesis in the presence or absence of arctigenin. The overexpression of Y371F-NFATc1 in BMMs neither induced osteoclastic differentiation nor rescued osteoclastogenesis inhibited by arctigenin (Fig. S3), suggesting that the phosphorylation status of Tyr-371 in

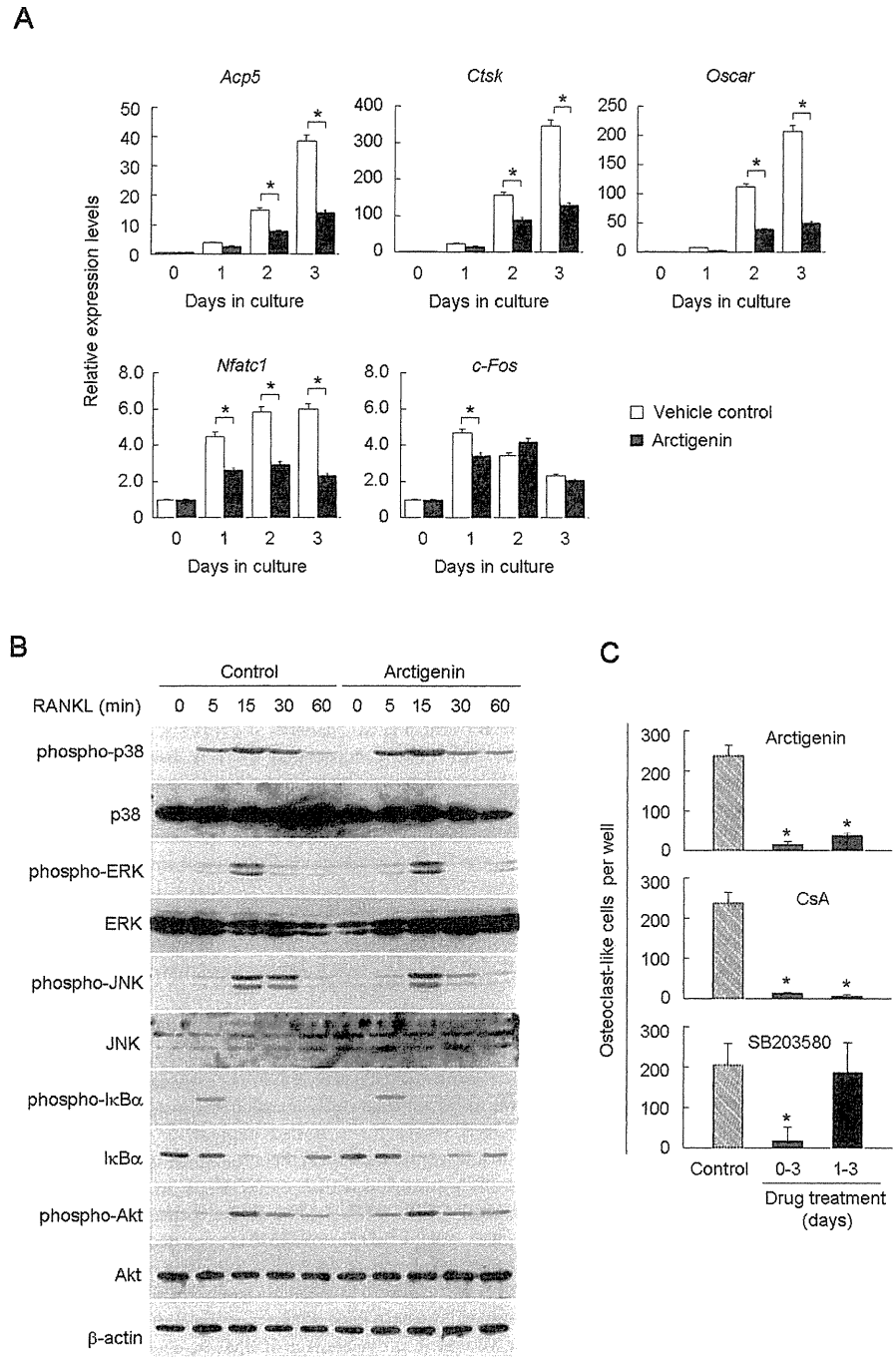

Figure 2. Effects of arctigenin on RANKL-induced signaling in BMMs. (A) Effects of arctigenin on the expression of osteoclast-related genes. BMMs were cultured in the presence of RANKL and M-CSF together with or without 1 μM arctigenin. After cultivation for the indicated periods, the expression of *Acp5*, *Ctsk*, *Oscar*, *Nfatc1*, and *c-Fos* mRNAs was analyzed by quantitative RT-PCR. Expression levels were normalized to *Gapdh* and expressed relative to day 0. Statistical analysis was performed between the control and arctigenin-treated values at indicated time points. (B) Effects of arctigenin on RANKL-induced signals in BMMs. BMMs were pretreated for 10 min with 1 μM arctigenin and further treated with RANKL. Whole cell lysates were harvested and analyzed by Western blotting with the indicated antibodies. (C) Effects of arctigenin, CsA, and SB203580 on osteoclast-like cell formation in BMM cultures. BMMs were cultured for 3 days in the presence of RANKL and M-CSF. BMM cultures were also treated with 1 μM arctigenin, 1 μg/mL CsA, or 1 μM SB203580 during days 0 – 3 and days 1 – 3. Cells were then fixed and stained for TRAP. TRAP-positive multinucleated cells containing more than three nuclei were counted as osteoclast-like cells. The results were expressed as means +/− SD (n = 3). *, $p<0.05$.

doi:10.1371/journal.pone.0085878.g002